GPO PRICE $ _____

CFSTI PRICE(S) $ _____

Hard copy (HC) 3.00

Microfiche (MF) .65

ff 653 July 65

NASA CR-72318

JULY 26, 1967

TOPICAL REPORT

COMPARISON OF DIRECT CONDENSING AND INDIRECT RADIATORS FOR NUCLEAR RANKINE SYSTEMS

by

R.D. Cockfield

R.E. Killen

prepared for

NATIONAL AERONAUTICS AND SPACE ADMINISTRATION

CONTRACT NASw-1449

ADVANCED NUCLEAR SYSTEMS OPERATION

GENERAL ELECTRIC

MISSILE AND SPACE DIVISION

KING OF PRUSSIA PARK

P.O. BOX 8661 · PHILADELPHIA, PENNA., 19101

NASA CR-72318
GE ANSO 6300-251
July 26, 1967

TOPICAL REPORT

COMPARISON OF DIRECT CONDENSING AND INDIRECT RADIATORS FOR NUCLEAR RANKINE SYSTEMS

by

R. D. Cockfield
R. E. Killen

prepared for

NATIONAL AERONAUTICS AND SPACE ADMINISTRATION

CONTRACT NASw-1449

Technical Management
NASA Lewis Research Center
Cleveland, Ohio
James P. Couch

ADVANCED NUCLEAR SYSTEMS OPERATION

GENERAL ELECTRIC
MISSILE AND SPACE DIVISION
KING OF PRUSSIA PARK
P.O. BOX 8661 · PHILADELPHIA, PENNA., 19101

NOTICE

This report was prepared as an account of Government-sponsored work. Neither the United States nor the National Aeronautics and Space Administration (NASA), nor any person acting on behalf of NASA:

A) Makes any warranty or representation, expressed or implied with respect to the accuracy, completeness, or usefulness of the information contained in this report or that the use of any information, apparatus, method, or process disclosed in this report may not infringe privately-owned rights; or

B) Assumes any liabilities with respect to the use of, or for damages resulting from the use of any information, apparatus, method or process disclosed in this report.

As used above, "person acting on behalf of NASA" includes any employee or contractor of NASA, or employee of such contractor, to this extent that such employee or contractor of NASA, or employee of such contractor prepares, disseminates, or provides access to, any information pursuant to his employment or contract with NASA, or his employment with such contractor.

Request for copies of this report should be addressed to:

NASA
Office of Scientific and Technical Information
Box 33
College Park, Md. 20740

ABSTRACT

A weight comparison is made between direct condensing radiators and indirect systems for nuclear potassium Rankine systems at a power level of 300 kWe and for meteoroid nonpenetration probabilities of 0.9, 0.99, and 0.999 for five years. The direct condensing radiators have a significant weight advantage for all conditions considered. However, consideration of startup requirements favor the indirect system and may offset the apparent advantage of the direct condensing system. The use of redundant loops in the indirect system provides a means of reducing radiator weight. A study is made to select the optimum redundancy arrangement.

TABLE OF CONTENTS

LIST OF ILLUSTRATIONS

LIST OF ILLUSTRATIONS (Cont)

LIST OF TABLES

1. SUMMARY

This report summarizes the results of the third of three tasks performed by the General Electric Company, Missile and Space Division, for the National Aeronautics and Space Administration under contract NASw-1449 - A Study of Radiator Structural and Mechanical Requirements.

The three tasks covered by this study are:

a. Definition of Spacecraft and Radiator Interrelations

b. Comparison of Load-Bearing and Non-Load-Bearing Radiators

c. Comparison of Direct Condensing and Indirect Radiators

Topical reports on the first two tasks have been issued as NASA CR-72245 and NASA CR - 72307, respectively.

The comparison made in this task of the study is for cylindrical beryllium radiators, applicable to a nuclear potassium Rankine system for an unmanned interplanetary probe mission, launched by a three-stage Saturn V. The power level is assumed to be 2.46 MWt heat rejected, approximately equivalent to 300 kWe net electrical power. Meteoroid nonpenetration probabilities of 0.9, 0.99 and 0.999 for a five-year life are considered.

The comparison shows that the direct condensing radiator has a significant weight advantage over the indirect condensing system; however, the scope of this study did not include the effects of startup requirements on the comparison. The weight advantage of the direct condensing system is approximately 70 percent at a probability of 0.9, decreasing to 23 percent as the probability increases to 0.999. Consideration of startup requirements, which favor the indirect system, may offset the apparent weight advantage of the direct condensing radiator. An evaluation of startup requirements was beyond the scope of this study.

The use of redundant loops in the indirect system provides a means of reducing radiator weight at the higher survival probabilities. As the degree of redundancy is increased, the increase in feed line weight and required area offset the reduction in armor weight. An optimum redundancy is therefore determined for each condition of survival probability.

The direct condensing radiators considered in this study were designed with the aid of the GE Spartan V computer code. The heat transfer and fluid flow relations used in the code show excellent correlation with available test data for potassium. Precautions are taken in the design of the direct condensing radiator to avoid problems of two-phase flow instability and maldistribution.

2. ASSUMPTIONS AND METHOD OF ANALYSIS

2.1 POWERPLANT SPECIFICATIONS

The radiators compared in this study are associated with a nuclear potassium Rankine power system used for unmanned missions. The parameters specified by NASA-Lewis, listed in Table 2-1, are consistent with the specifications used in the comparison of load-bearing and non-load-bearing concepts from the second task of this contract, reported in Reference 2-1. For simplicity, and for comparison with previous studies, the efficiency of the power system was assumed to be such that the net electrical power is 300 kWe. Throughout this report, the power level is referred to by this electrical power, rather than by the thermal power rejected by the radiators.

The pump penalty specified for the indirect system is used to account for the pump work in optimizing the radiator design (Table 2-1). The specified value of 25 lb/kWe is typical of a potassium Rankine system with a beryllium radiator. Note that the assumptions used for the systems compared in the previous task of this study lead to somewhat higher penalties. However, the magnitude of the penalty is not critical, since the pump work has only a secondary effect in determining the optimum radiator weight.

Radiator construction was assumed to consist of beryllium armor and fins and stainless steel tubes, headers and feed lines. Assuming an emittance of 0.90, an absorptance of 0.75, and an incident flux of 440 Btu/hr-ft^2, the effective sink temperature is 52°F. At the radiator temperatures of interest in this study, the sink temperature has little influence on thermal performance. As heliocentric distance increases during an interplanetary probe mission, the effective sink temperature decreases and becomes even less significant. The conservative assumption is made that the powerplant will be operated initially at full power in earth orbit so that near-earth incident fluxes are assumed for the thermal analysis.

TABLE 2-1. SPECIFIED RADIATOR PARAMETERS

	DIRECT	INDIRECT
Coolant	K	Nak
Inlet Temperature	1350° F	1300° F
Heat Rejected	2.46 MW_t	2.46 MW_t
Life	5 years	5 years
Pump Efficiency		20%
Power Penalty		25 lb/kWe
Meteoroid Nonpenetration Probability	0.9 0.99 0.999	0.9 0.99 0.999
Launch Vehicle	Three-Stage Saturn V	Three-Stage Saturn V

The circuit schematics for the two radiator types being compared are shown in Figure 2-1. The direct condensing radiator eliminates the need for a condenser-heat exchanger, and for the pumps in the heat rejection loops of the indirect condensing radiator. The weight of these components is included in the comparison. Cycle conditions through the turbine and boiler feed jet pumps are assumed to be the same in both cases.

The powerplant conditions which were fixed in this study were the fluid turbine exit conditions and the fluid temperature to the electromagnetic pump. Fluid temperature at turbine exit was specified to be 1350°F; the value for fluid quality was taken as 83.8 percent. The fluid temperature to the EM pump, which is of minimal importance to the radiator design and weight, was arbitrarily chosen to be 1100° F.

2.2 METEOROID CRITERIA

The meteoroid criteria used to determine armor thickness for the radiators compared in this study are based on the relations derived by Loeffler, Lieblein, and Clough (Reference 2-2); these relations are described more fully in Reference 2-1. As in the analysis presented in Reference 2-1, a damage thickness factor of 1.75 was assumed,

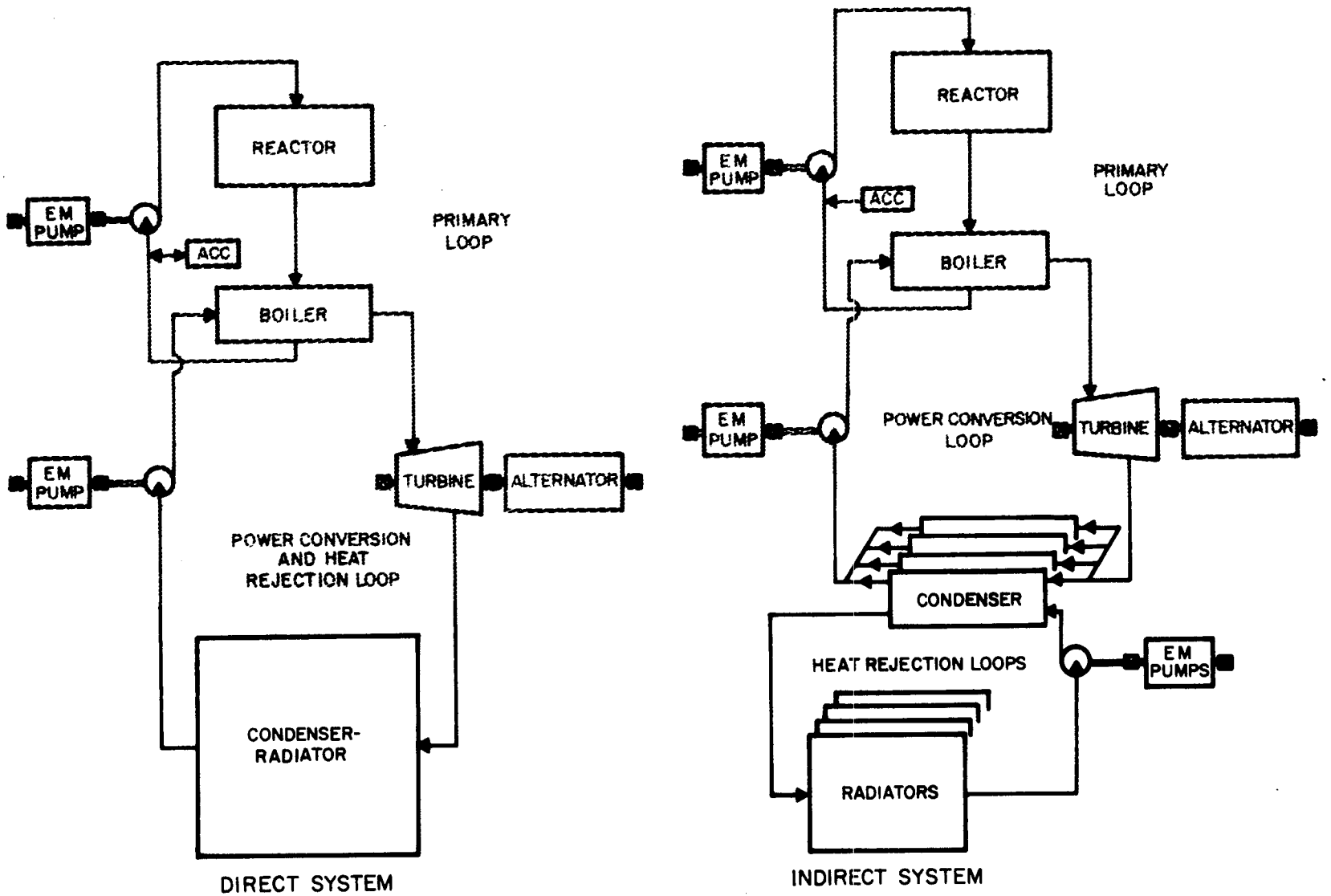

Figure 2-1. Schematics of Direct and Indirect Heat Rejection Systems

which corresponded to a dimple height of 20-percent, and the cratering coefficient for beryllium armor was assumed to be 2.28.

Three values of nonpenetration probability were specified in Table 2-1 to assess the sensitivity of the radiator weights to meteoroid criteria. Note in comparing the results of this study with previous radiator weight estimates that the meteoroid criteria are more severe than those used in the past. Table 2-2 compares the current criteria with those used in the Navigator Studies of 1964 (Reference 2-3). The reduction in average meteoroid velocity and the increase in meteoroid density have a combined effect of decreasing the armor thickness required by 22-percent. However, the longer survival time and higher nonpenetration probability, equivalent to an increase in the mean time to failure by a factor of 219, have a net effect of increasing the armor thickness by a factor of 5.34.

An advantage of the indirect condensing system is that, for a single set of turbomachinery, multiple heat rejection loops can be used. By providing redundancy in the number of independent heat rejection loops, a reduction in the armor thickness required can be obtained, which often results in a reduction in radiator weight. To determine the degree of redundancy resulting in minimum radiator weight, a study of redundancy was made for the indirect radiators used in the comparison of this study. The results of this study are presented in Section 3. The effect of providing redundancy on the survival probability of the system is determined by solving the binomial distribution equation:

$$S = \sum_{r=r_s}^{r=n} \frac{n!}{(n-r)!\ r!} P^r\ (1-P)^{n-r} \qquad (2\text{-}1)$$

where:

- S = nonpenetration probability of system
- P = nonpenetration probability of individual loops
- n = number of loops provided
- r_s = number of loops surviving

TABLE 2-2. METEOROID CRITERIA COMPARISON

	NAVIGATOR (1964)	CURRENT
Meteoroid Velocity (km/sec)	30	20
Meteoroid Density (g/cc)	0.44	0.50
Survival Time	10,000 hr	5 yr
Survival Probability	0.95	0.999
Mean Time to Failure (hr)	0.2×10^6	43.8×10^6
Relative Armor Thickness	1	5.34

Table 2-3 lists typical solutions for a required nonpenetration probability of 0.999. As an illustration, if six heat rejection loops are provided and survival of only five loops is required to provide full power capacity, the nonpenetration probability required of each loop is 0.9918, compared with 0.9998 if all six are required to survive. The armor thickness is computed for the entire system on the basis of P^n. Therefore, the reduction in armor thickness t that has been obtained by the use of redundancy is:

$$\frac{t}{t_o} = \left(\frac{\ln S}{\ln P^n}\right)^{0.2488} = \left(\frac{\ln 0.999}{\ln 0.9918^6}\right)^{0.2488} = 0.38 \qquad (2\text{-}2)$$

that is, the armor thickness is only 38-percent of that required with no redundancy, while the radiator area is greater by 20-percent. The net effect on radiator weight may be an increase or a decrease, depending on how much of the radiator weight is in the armor.

2.3 SPACECRAFT CONFIGURATION

The radiators compared in this study, both the direct and indirect condensing types, are assumed to be non-deploying, load-bearing types, conical in shape, and fitting within a 10-degree half-cone angle. For the direct condensing radiators considered in

this study, it was found that the area available on a conical surface of 10-degree half-cone angle having a base diameter of 260 inches is less than that required for heat rejection capability. The payload section is therefore assumed to be of the necessary length to act as an adapter section. The half-cone angle was chosen on the basis of studies reported in Reference 2-4, which showed that the 10-degree angle favors both low shield weight and low launch loads. In the comparisons made in this study, however, these factors are of secondary significance.

The feed line network for the radiators compared in this study was assumed to be as shown in Figures 2-2 and 2-3. For the indirect condensing radiators, the feed line lengths were determined by an iterative process. The lengths were first determined for a nominal radiator area of 1000 square feet. For each condition of redundancy, the optimum radiator area was then determined using these lengths. The area was compared with 1000 square feet and the feed line lengths adjusted accordingly. A new optimum area was then determined and the comparison repeated until the feed line lengths were consistent with the calculated radiator area. Although the weight adjustments made by each iteration were small, the procedure was necessary to properly identify the optimum degree of redundancy and to determine accurately the weight differences in the comparison.

2.4 CONDENSING RADIATOR ANALYSIS

The analysis of condensing radiators involves virtually all of the problems encountered in the analysis of non-condensing radiators. In addition, there are several fundamental characteristics, adding to the complexity of the analysis which warrant some discussion.

2.4.1 CONDENSING HEAT TRANSFER RELATIONS

The temperature drop from the bulk fluid to the tube wall is generally more difficult to calculate for condensing systems than for systems employing liquid working fluids. For condensing radiators using potassium in the 1300° F range, this temperature drop is small. As a result it has been neglected in many of the previous studies of

TABLE 2-3. SURVIVAL PROBABILITY OF EACH LOOP FOR A SYSTEM SURVIVAL PROBABILITY OF 0.999

NUMBER PROVIDED (n)	NUMBER SURVIVING (r_s)											
	1	2	3	4	5	6	7	8	9	10	11	12
1	0.999											
2	0.9683	0.9995										
3	0.9000	0.9816	0.9997									
4	0.8222	0.9360	0.9870	0.9997								
5		0.8780	0.9525	0.9899	0.9998							
6		0.8185	0.9061	0.9621	0.9918	0.9998						
7		0.7625	0.8563	0.9234	0.9684	0.9930	0.9998					
8			0.8073	0.8804	0.9351	0.9730	0.9940	0.9998				
9			0.7612	0.8371	0.8975	0.9438	0.9764	0.9947	0.9999			
10			0.7184	0.7953	0.8587	0.9102	0.9504	0.9789	0.9952	0.9999		
11				0.7559	0.8206	0.8751	0.9201	0.9555	0.9810	0.9957	0.9999	
12				0.7192	0.7841	0.8401	0.8880	0.9279	0.9598	0.9827	0.9960	0.9999

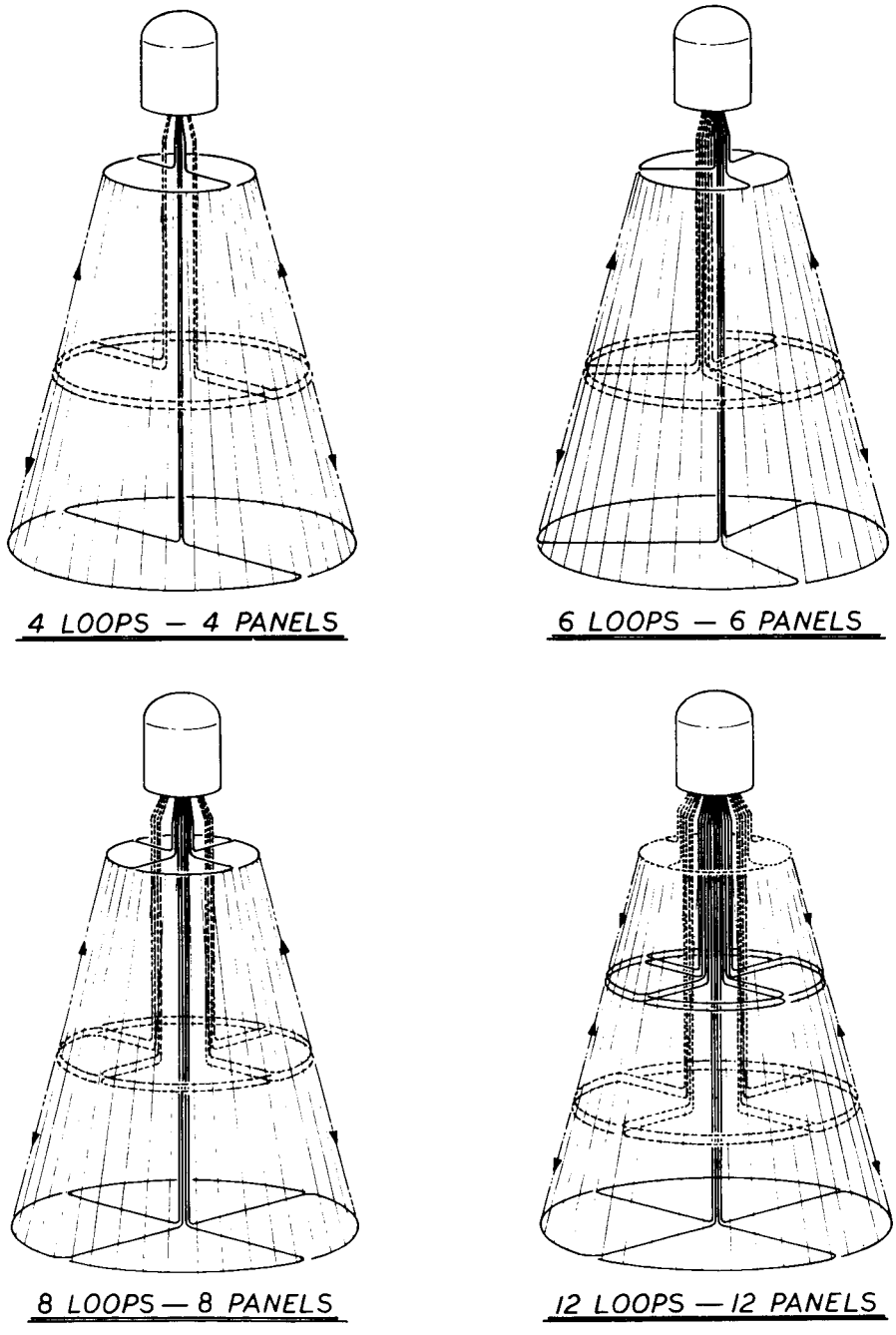

Figure 2-2. Feed Line Networks for Indirect Condensing Radiators

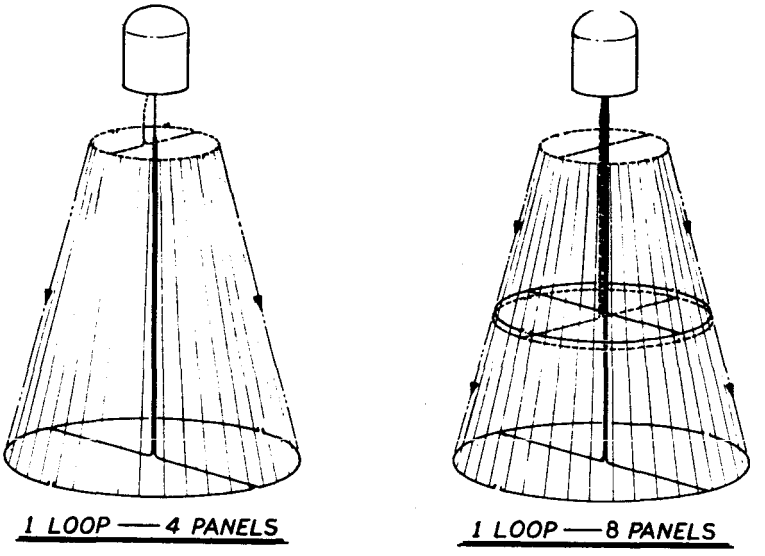

Figure 2-3. Feed Line Networks for Direct Condensing Radiators

condensing radiators, such as those of Denington (Reference 2-5), Haller (Reference 2-6), Krebs (Reference 2-7), and Stone (Reference 2-8). Neglect of this temperature drop results in an underestimate of the required radiator area of only two to three percent. However, in the analysis performed for this study, this temperature drop was included, not only to improve accuracy, but to insure flexibility in the method of analysis to include cases where this temperature drop is not negligible.

In recent years, the evaluation of condensing heat transfer coefficients for liquid metals has received widespread attention. As a result, reliable data are available for various liquid metals and specifically for potassium which is of interest for high-temperature Rankine power systems.

The correlation used in this study to predict condensing heat transfer coefficients is a modification of Nusselt's relation:

$$\frac{\bar{h}_c}{k_f}\left[\frac{\nu^2}{g_c}\right]^{1/3} = 1.47\ N_{Re}^{-1/3} \qquad (2\text{-}3)$$

where $\bar{h}_c$ = average condensing heat transfer coefficient from fluid inlet to point of complete condensation

k_f = thermal conductivity in the film

ν = kinematic viscosity

g_c = gravitational constant

N_{Re} = Reynold's number

Nusselt's relation tends to overestimate liquid metal condensing coefficients, but for many fluids it provides good agreement with experiment.

The Spartan V code, which is the principal tool used in the condensing radiator analysis, uses a variation of the Nusselt relation in order to increase its applicability to different systems. This relation uses a multiplier to adjust Nusselt's relation to liquid metal experimental data in the following manner:

$$\frac{\bar{h}_c}{k_f}\left[\frac{\nu^2}{g}\right]^{1/3} = \left[1.47\ N_{Re}^{-1/3}\right] C_c \qquad (2\text{-}4)$$

Based on the work of Sawochka (Reference 2-9), the appropriate value for C_c for potassium is 0.5 (See Figure 2-4). The experimental evaluation of potassium condensing coefficients by Sawochka is an important step in the understanding of the alkali metal condensing process and in the engineering development of the nuclear potassium Rankine power system. A brief outline of this work is given in the following paragraphs.

Nusselt's condensing model neglected the effects of interfacial shear stress, turbulent transports and a vapor phase thermal resistance. Sawochka attributed the observed deviations from Nusselt's relation to the existence of a vapor phase thermal resistance which was due to the non-ideality of the potassium vapor. The non-ideal behavior is due to the formation of dimers and tetramers as well as the monomer in gaseous potassium. Evidence for the existence of these species was shown by Ewing (Reference 2-10). The effect of the non-ideal behavior manifests itself at low pressures (below 2 psia), in which regime Sawochka observed a sharp decrease in the overall condensing heat transfer coefficient.

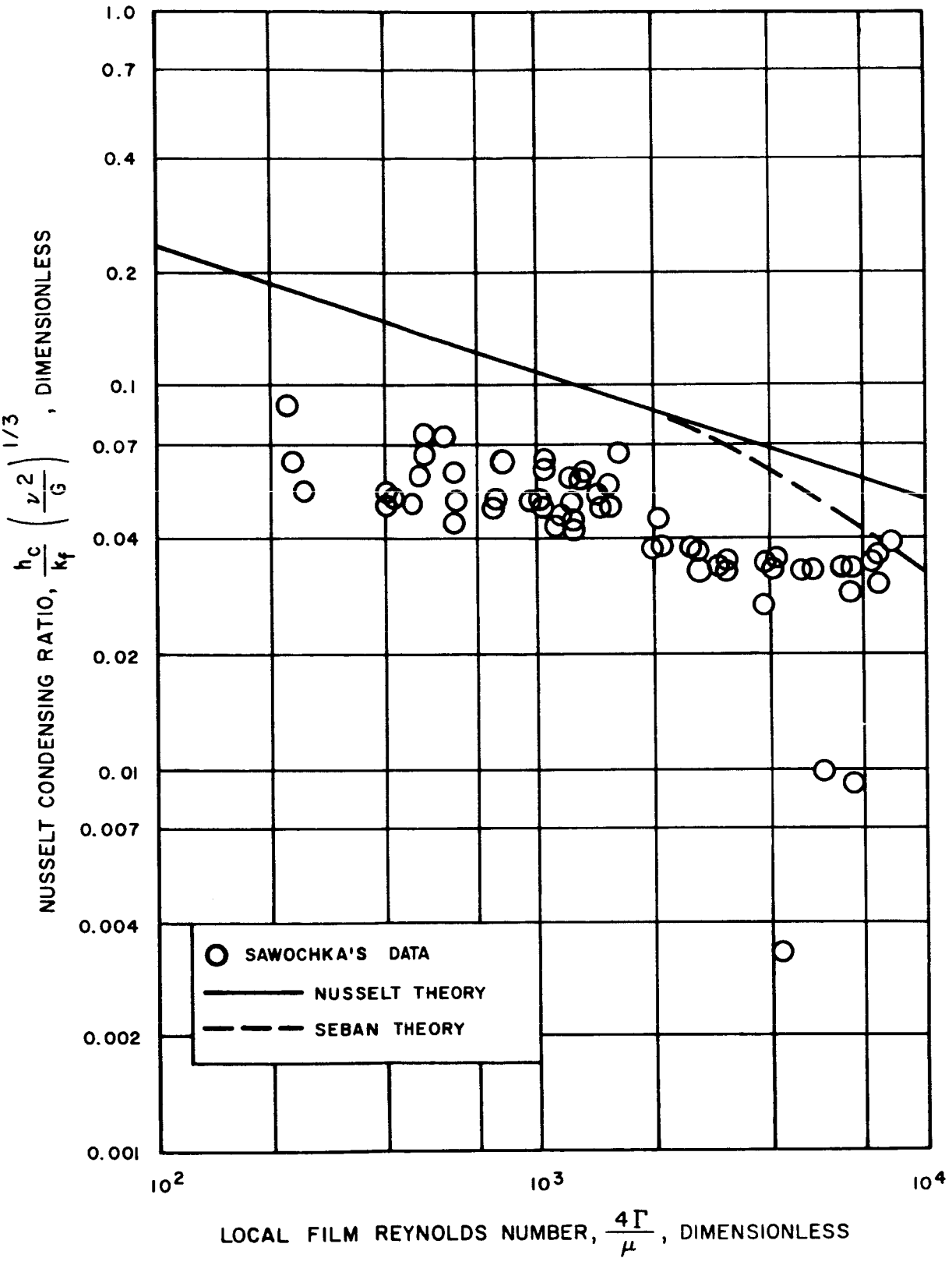

Figure 2-4. Comparison of Sawochka's Experimental Data for Potassium to the Nusselt Relation

The condensing local heat transfer coefficient is defined by Sawochka as:

$$\frac{1}{h_c} = \frac{1}{h_f} + \frac{1}{h_v} \qquad (2\text{-}5)$$

where h_f = heat transfer coefficient in the film

h_v = heat transfer coefficient in the vapor

The liquid film thermal resistance, $1/h_f$, was predicted by using film thicknesses given by Dukler (Reference 2-11). Assuming a linear temperature profile:

$$h_f = k_f/\delta \qquad (2\text{-}6)$$

where δ = condensate film thickness

It remains to develop an expression for the vapor phase thermal resistance which will fit the data obtained by subtracting the predicted liquid film thermal resistance from the measured overall thermal resistance. For an ideal gas in equilibrium with its liquid, the rate at which molecules impinge on the liquid surface is equal to the rate at which molecules leave the liquid. From the kinetic theory of gases, this situation is described by the following relationship:

$$P_l \left[\frac{M}{2\pi R T_l}\right]^{1/2} = P_v \left[\frac{M}{2\pi R T_v}\right]^{1/2} \qquad (2\text{-}7)$$

where P = pressure

M = molecular weight

R = universal gas constant

T = temperature

v = subscript for vapor

l = subscript for liquid

If there is a net mass transfer of vapor into the liquid, which is the case during condensation, the dynamic equilibrium is upset; therefore:

$$\frac{W}{A} = P_v \left[\frac{M g_c}{2\pi R T_v}\right]^{1/2} - P_l \left[\frac{M g_c}{2\pi R T_l}\right]^{1/2} \qquad (2\text{-}8)$$

where W = flow rate

A = area

g_c = gravitational constant

For a non-ideal gas Equation 2-8 must be changed to the following:

$$\frac{W}{A} = \sigma_c P_v \left[\frac{M g_c}{2\pi R T_v}\right]^{1/2} - \sigma_e P_l \left[\frac{M g_c}{2\pi R T_l}\right]^{1/2} \qquad (2\text{-}9)$$

where σ_c = condensation coefficient

σ_e = evaporation coefficient

By equating the condensation coefficient to the evaporation coefficient, it can be shown that:

$$\frac{q}{A \Delta T} = h_v = \sigma_c K \left[\frac{M g_c}{2\pi RT}\right]^{1/2} \left[\frac{dP}{dT} - \frac{P}{2T}\right] \qquad (2\text{-}10)$$

where g = WK

ΔT = temperature drop

K = latent heat of vaporization

The experimental data is shown to correlate fairly well over the temperature range by using a value of 0.2 for the condensation coefficient σ_c (See Figure 2-5). Although there is no strong argument for equating σ_e to σ_c, the treatment provided by Sawochka gives a better understanding of the condensing process and satisfies the experimental data.

2.4.2 TWO-PHASE FLOW PRESSURE DROP

Since the effective temperature of a condensing radiator is dependent upon the static pressure of the condensing fluid, accurate two-phase flow pressure drop predictions are necessary for proper radiator design. The complexity of the two-phase flow process, which may assume different flow patterns (that is, fog, bubble, slug, annular, etc.) under various conditions, makes the formulation of an analytical model extremely difficult (See Figure 2-6). The most widely cited analytical work in this

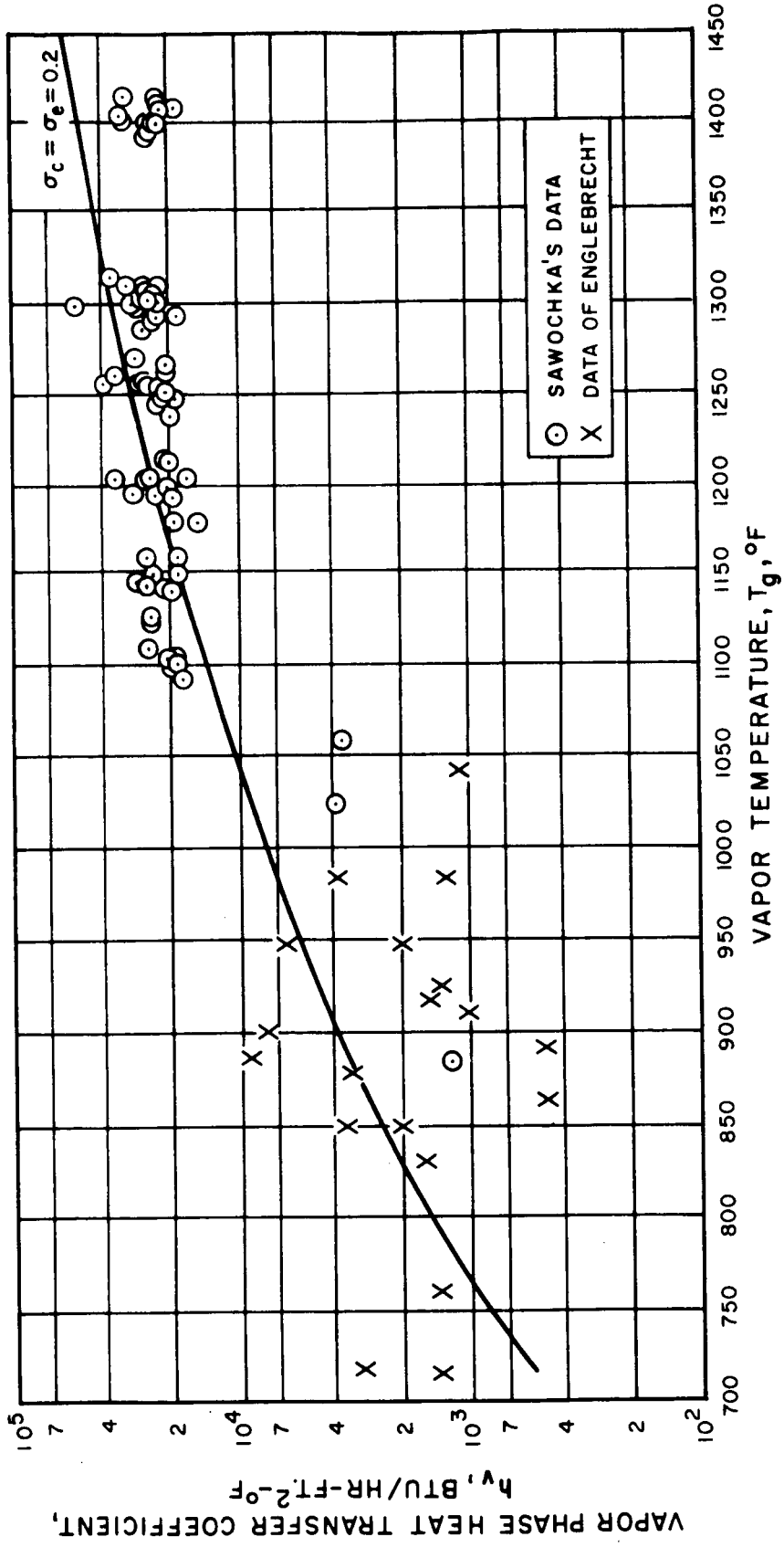

Figure 2-5. Comparison of Vapor Heat Transfer Results with Kinetic Theory Prediction (from Sawochka)

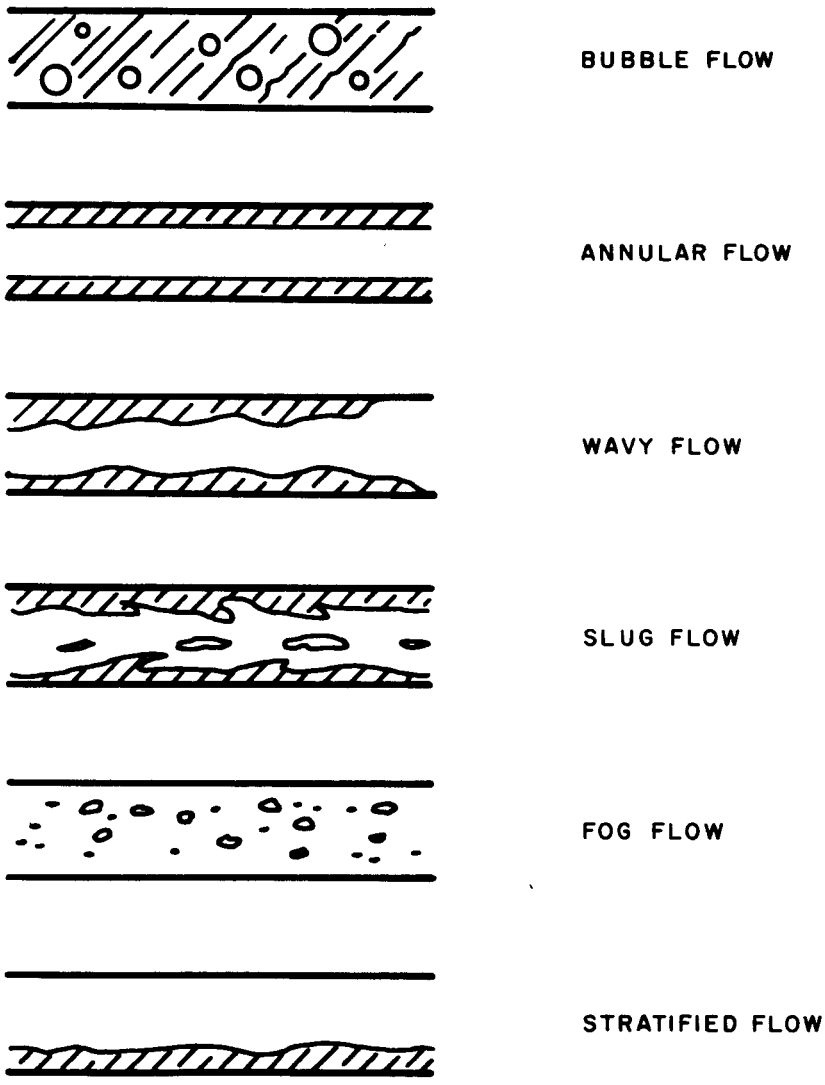

Figure 2-6. Two-Phase Flow Regimes

area is that of Lockhart and Martinelli (Reference 2-12) who were able to achieve mild agreement between their experimental and analytical efforts.

The two-phase flow pressure drop can be expressed in terms of the frictional pressure drop and the pressure rise due to momentum changes:

$$\Delta P_{tp} = \Delta P_f + \Delta P_m \tag{2-11}$$

The momentum term is expressed by the following equation:

$$\Delta P_m = \frac{\rho v_o^2}{g_c} \tag{2-12}$$

where ρ = density

v_o = inlet vapor velocity

The equation used for calculating the frictional two-phase flow pressure drop is given by the Lockhart and Martinelli relation as:

$$(\Delta P/\Delta L)_f = \varphi_v^2 \ (\Delta P/\Delta L)_v \tag{2-13}$$

where $(\Delta P/\Delta L)_v$ is the pressure drop per unit length if the vapor phase were assumed to flow alone. The variable φ_v was correlated to a parameter X which was defined as:

$$X^2 = \left(\frac{4}{\pi D}\right)^{m-n} \frac{C_l}{C_v} \frac{W_l^{2-n}}{W_v^{2-m}} \frac{\rho_v}{\rho_l} \frac{\mu_l^n}{\mu_v^m} \tag{2-14}$$

where C = constant used in Blasius equation

μ = viscosity

D = pipe diameter

which is equal to the ratio of the liquid to the gaseous pressure drop if each phase were assumed to flow separately. The exponents m and n are dependent upon the type

of flow present; for turbulent-turbulent flow (turbulent in both the liquid and vapor phases), Lockhart and Martinelli reduced the above equation to:

$$X_{tt}^2 = \left(\frac{W_l}{W_v}\right)^{1.8} \frac{\rho_v}{\rho_l} \left(\frac{\mu_l}{\mu_v}\right)^{0.2} \qquad (2\text{-}15)$$

where $m = n = .2$

Experimental curves for φ_v versus X were presented by the experimenters to provide a means of calculating two-phase flow pressure drops. Lockhart and Martinelli suggested that this method could be used for all flow patterns except slug flow; however, the correlation has been shown to differ by as much as 250 percent from experiment.

McMillan, Fontaine and Chaddock (Reference 2-13) proposed a modification to the Lockhart and Martinelli correlation which included the effect of the interfacial shear between the two phases in determining the pressure drop. McMillan et al pictured the gas phase as flowing in an annulus surrounded by liquid; the interfacial waves are thought of as forming a "rough wall." Confining themselves only to the turbulent-turbulent case, McMillan et al used the approach outlined below.

As previously stated, the Lockhart-Martinelli correlation is defined as:

$$(\Delta P/\Delta L)_f = \varphi_v^2 \left(\Delta P / \Delta L\right)_v = \varphi_v^2 \; 2 f \rho_v v_v^2 / D g_c \qquad (2\text{-}16)$$

where the friction factor, f is expressed in the Blasius form:

$$f = C / N_{Re}^m \qquad (2\text{-}17)$$

The values used by Lockhart and Martinelli for turbulent-turbulent flow were $C = 0.046$ and $m = 0.2$, which correspond to smooth pipes. In order to account for interfacial roughness, McMillan et al, using dimensional analysis, defined a new variable θ, which is the ratio of vapor Reynolds number to Weber number. Theta is the ratio of

surface tension to viscous forces and includes all the important parameters affecting interfacial surface roughness; it is written as:

$$\theta = \sigma g_c \Big/ \mu_v \qquad (2\text{-}18)$$

It was assumed that the interfacial roughness could be measured in terms of C which was postulated to be a function of θ. Experimental work was performed to obtain the relationship between C and θ using the gas and liquid phases of trichloromonofluouromethane. The value of C obtained can be expressed in terms of the experimental measurement for $(\Delta P/\Delta L)_{tp}$ and the Lockhart-Martinelli formulation. Using Equations 2-16 and 2-17:

$$C_{exp} = \frac{[(\Delta P/\Delta L)_f]_{exp} \quad (0.046)}{(\Delta P/\Delta L)_v \quad \varphi_v^2} \qquad (2\text{-}19)$$

The results obtained from this treatment are as follows:

$$\begin{aligned} \theta &\leq 57.23 && C = 0.10 \\ 57.23 \leq \theta &\leq 327.59 && C = 4.182\,\theta^{-0.9225} \\ \theta &\geq 327.59 && C = 0.02 \end{aligned}$$

For the data examined, the analytical predictions by McMillan et al resulted in an accuracy of ±10 percent as compared to +56 to -35 percent by the Lockhart-Martinelli correlation.

The proposed "rough wall model" modification of the Lockhart-Martinelli correlation is used in this study and efforts have been made to judge its applicability to two-phase flow pressure drop measurement for liquid metals by comparison with experimental data. Gutierrez, Sekas, Acker and Fenn (Reference 2-14) have conducted experiments with potassium condensing in a radiator panel over a range of fluid temperatures from 1200 to 1500° F. The panel consisted of cylindrical inlet and outlet headers (3.5-inch ID, 4.0-inch OD) which were joined by nine parallel flow tubes using a central fin geometry; 316 stainless steel was used throughout. The tubes had an inside diameter

of 0.500 inches and an outside diameter of 1.34 inches; fins were 0.080 inches thick and 0.90 inches long. A separation distance of 0.125 inches was kept between fins. Environmental pressure was kept at 3×10^{-3} torr and the sink temperature was below 300°F during the radiator test. Analysis was performed using these test conditions and assuming a vapor inlet quality of 88 percent.

To perform the analysis, the Spartan V computer code (to be discussed more fully later) was used. The results of the study are shown in Figures 2-7 through 2-12 for fluid inlet temperatures of 1235, 1350, and 1420°F. Figures 2-7 through 2-9 show the variation of static pressure drop with the inlet vapor flow rate.

McMillan's modification of the Lockhart-Martinelli correlation gives excellent agreement over the range of inlet vapor flow rates for the inlet temperatures of 1235 and 1420°F. For the inlet vapor temperature of 1350 the analytical curve is lower than the best fit through the data. Personal communication with O. A. Gutierrez of NASA-Lewis, however, revealed that the data at 1350°F is of a preliminary nature and that a final report on the test is in preparation. Figures 2-10 through 2-12 show the variation of condensing length with inlet vapor flow rate. Also shown are the analytical results predicted by Gutierrez et al and by Spartan V. Since no attempt was made by the experimenters to include the axial fluid temperature drop due to the static pressure change, their predicted condensing lengths are less accurate at the high flow rate conditions.

The close agreement shown between Spartan V and the experimental results seem to demonstrate the applicability of the modified Lockhart-Martinelli correlation to liquid metal two-phase flow.

2.4.3 FLOW STABILITY

Necessary to successful direct condensing radiator design is the ability to maintain a constant flow of fluid, free of any instabilities. Inherent in this requirement is the ability of the condensing fluid to maintain a single flow pattern under any external or internal perturbations to which the system is subjected. Different flow patterns result in different fluid inventories in the condensing tube which causes a shift in the

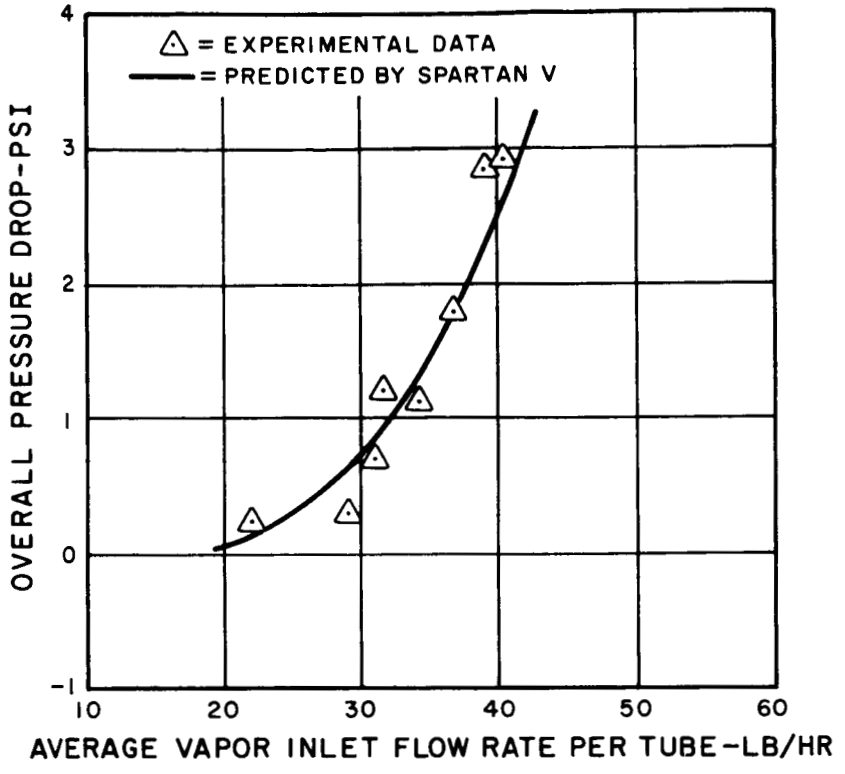

Figure 2-7. Pressure Drop Comparison, Vapor Header Temperature 1235° F.

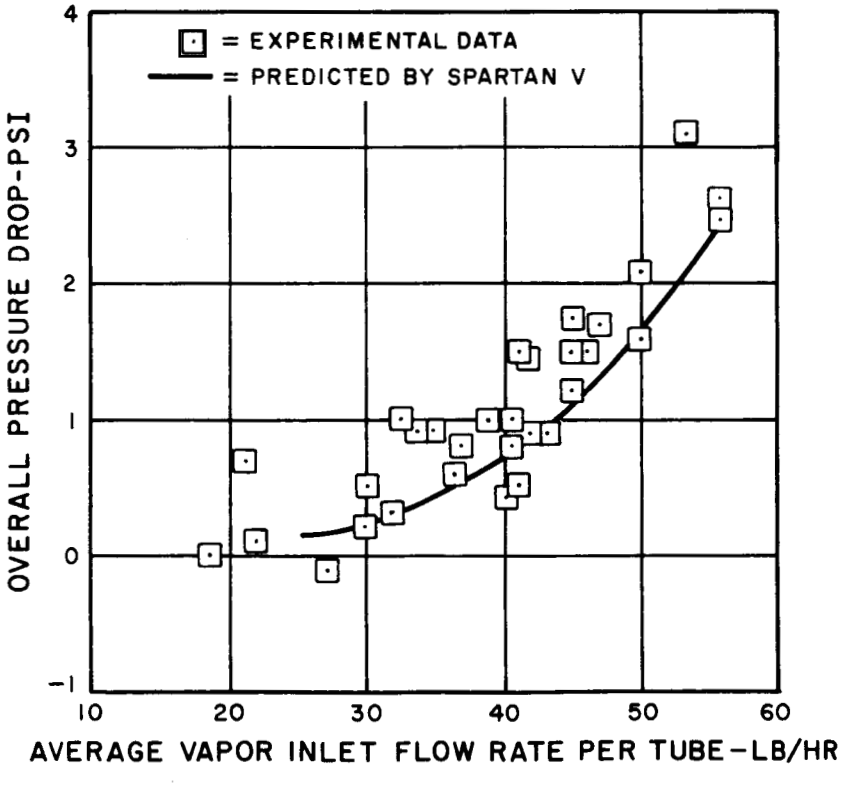

Figure 2-8. Pressure Drop Comparison, Vapor Header Temperature 1350° F.

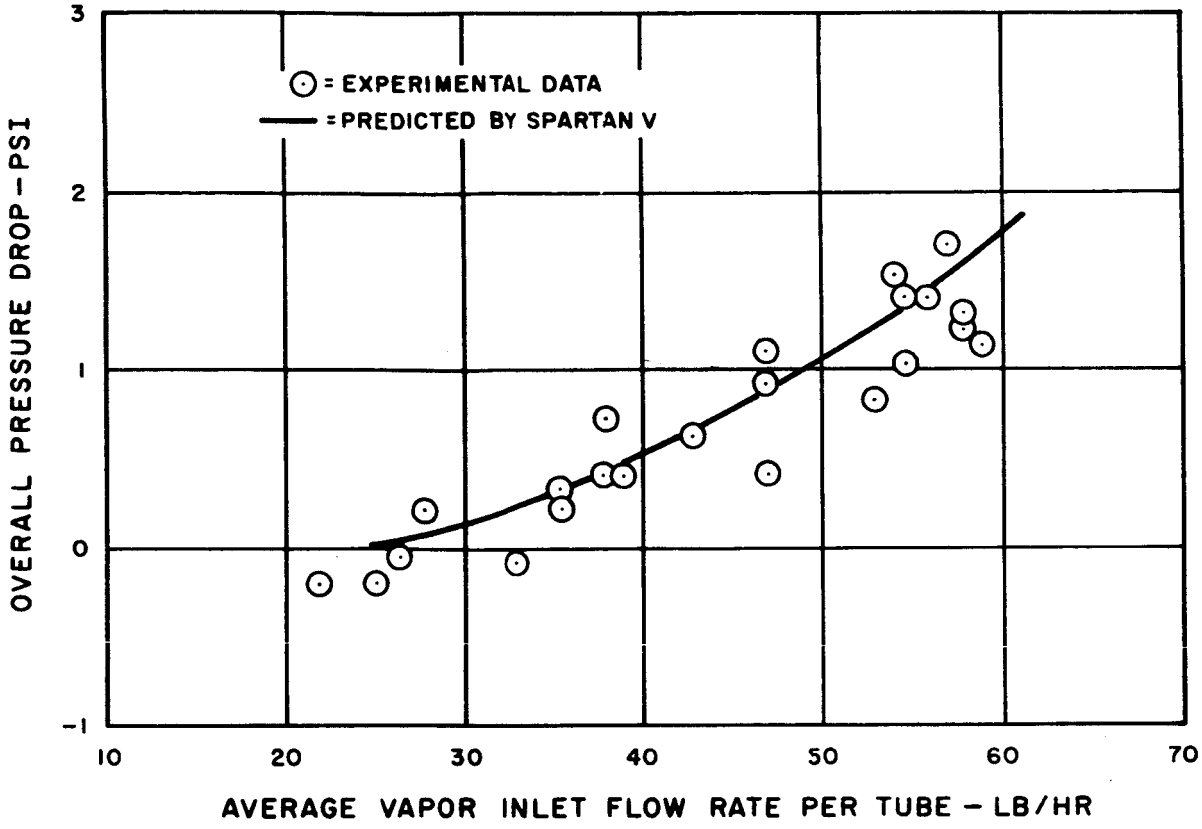

Figure 2-9. Pressure Drop Comparison, Vapor Header Temperature 1420°F.

vapor-liquid interface. A stable vapor-liquid interface is the controlling factor in producing dependable and predictable condensing radiator performance.

The flow instabilities pertinent to condensing radiators are interfacial instability, runback instability, liquid leg instability and zero-g instability. These forms of two-phase flow instabilities have been examined analytically and experimentally by various investigators, notably V. H. Heiskala, R. C. Smith, E. A. Elliott and R. T. Lancel (Reference 2-15) under the Mercury Rankine Program (SNAP-2).

Interfacial instability is the inability of the fluid to form a stable meniscus which separates the condensing and subcooling portions of the tube (See Figure 2-13). The stability of the meniscus is dependent upon surface tension energy and the kinetic and potential energy of the disturbing wave. The total energy per wavelength of a wave, E/λ, is given by Lamb (Reference 2-16) as:

$$\left(E/\lambda\right)_{KE+PE} = g/g_c \left[\frac{\left(\rho_l - \rho_v\right)\eta_o^{\,2}}{2}\right] \qquad (2\text{-}20)$$

where η_o = maximum wave amplitude

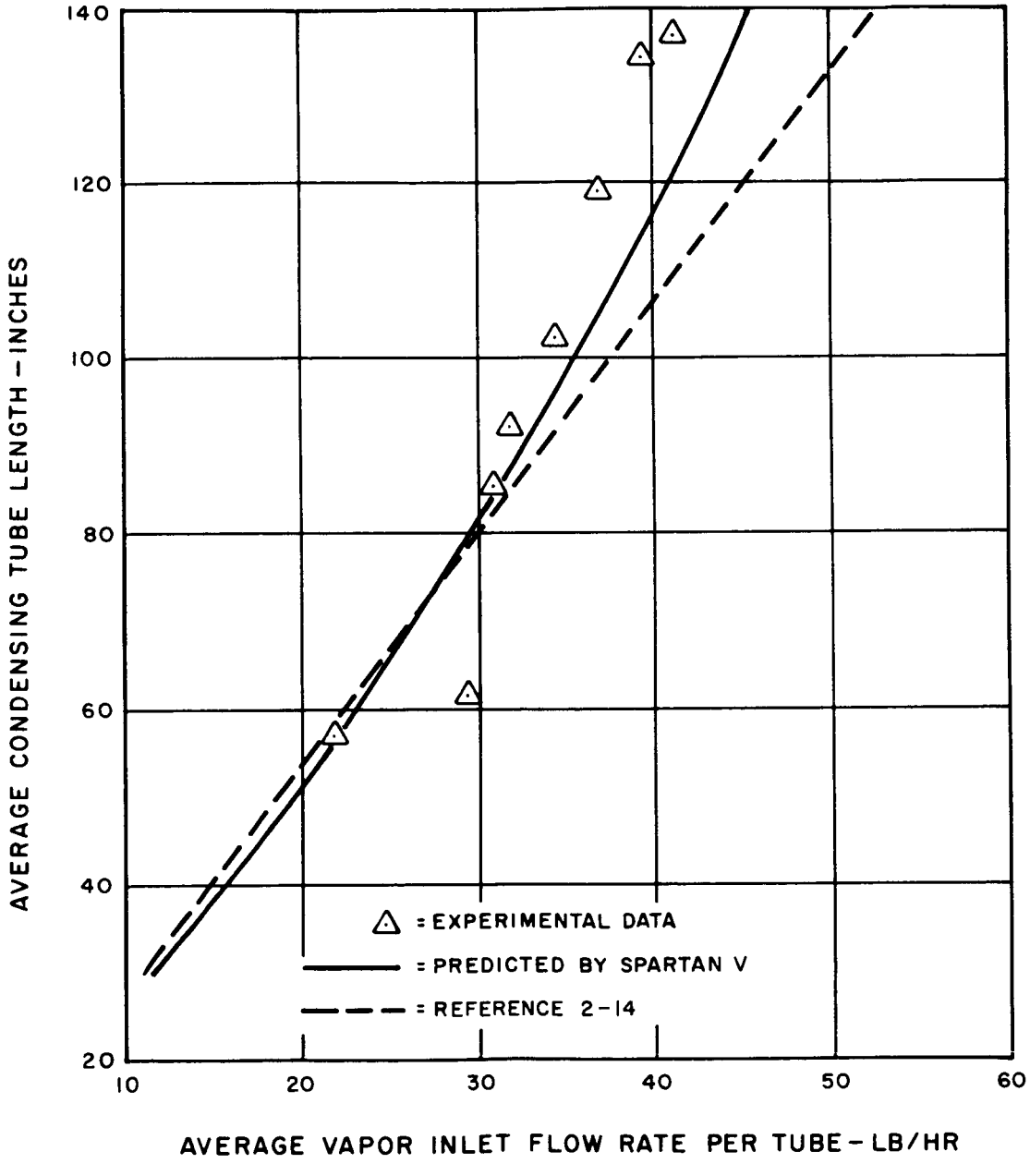

Figure 2-10. Condensing Tube Length Comparison, Vapor Header Temperature 1235°F.

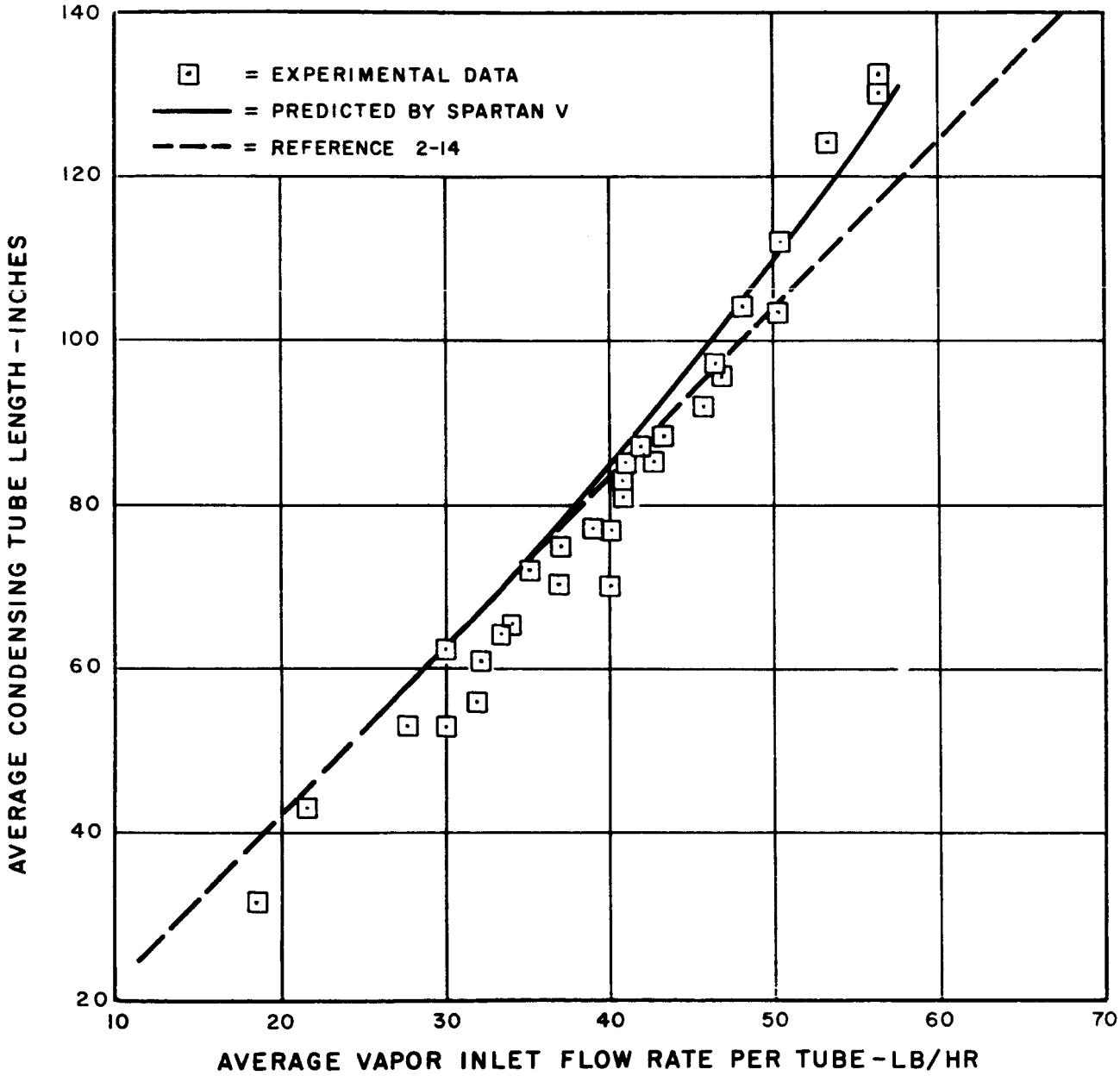

Figure 2-11. Condensing Tube Length Comparison, Vapor Header Temperature 1350°F.

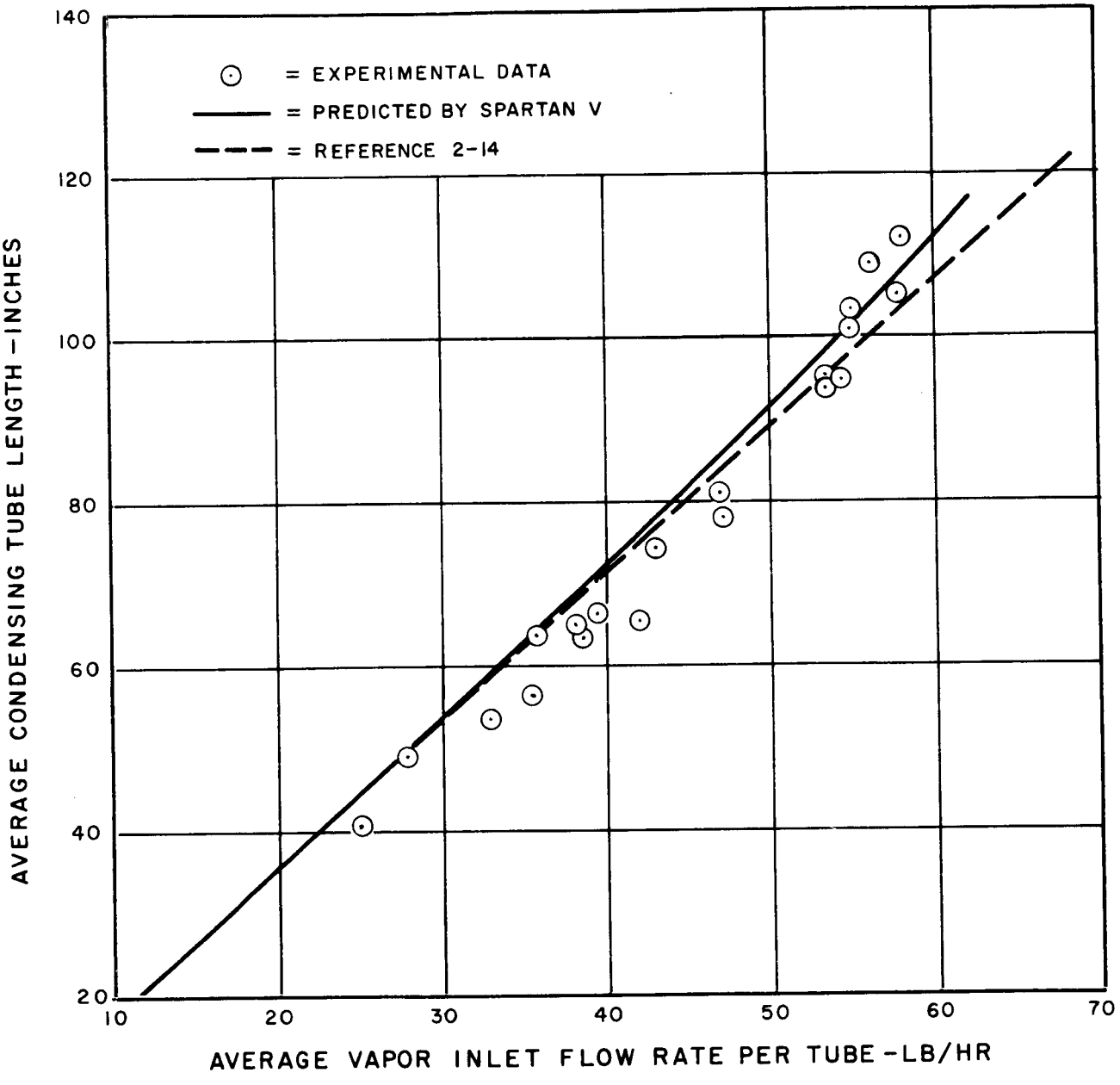

Figure 2-12. Condensing Tube Length Comparison, Vapor Header Temperature 1420°F.

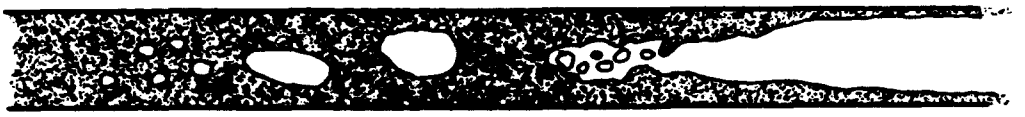

Interfacial Instability Present

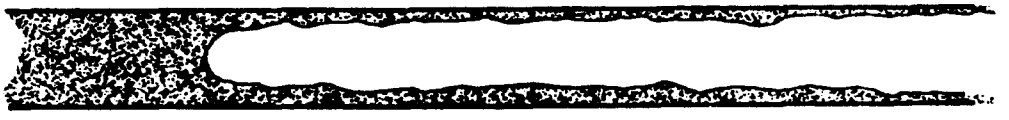

Annular Flow with Stable Interface

Figure 2-13. Condensing Tube Fluid Profiles

By integrating along the length of the wave, the surface tension energy per wavelength is:

$$\left(E/\lambda\right)_{\substack{\text{Surface}\\\text{Tension}}} = 1/\lambda \int_{o}^{\lambda} \Delta P \, \eta \, dx \qquad (2\text{-}21)$$

Assuming a sine wave form and taking a force balance at the vapor-liquid wave interface, Equation 2-21 is shown by Tong (Reference 2-17) to reduce the following:

$$\left(E/\lambda\right)_{\substack{\text{Surface}\\\text{Tension}}} = 2\sigma \left(\frac{\pi \eta_o}{\lambda}\right)^2 \qquad (2\text{-}22)$$

where σ = Surface tension

In order for the wave to damp out, the surface tension energy must be greater than the sum of the potential and kinetic energies. Therefore, the longest stable wavelength is:

$$\lambda = 2\pi \sqrt{\frac{\sigma}{\left(\rho_l - \rho_v\right) g/g_c}} \qquad (2\text{-}23)$$

For cylindrical geometry, the stable wavelength can be related approximately to a critical diameter:

$$D_c = \pi \sqrt{\frac{\sigma}{\left(\rho_l - \rho_v\right) g/g_c}} \qquad (2\text{-}24)$$

Consideration of the contact angle between the liquid and the tube walls leads to the following conservative relationship when the contact angle is zero or 180 degrees:

$$D_s = 1.835 \sqrt{\frac{\sigma}{\left(\rho_l - \rho_v\right) g/g_c}} \qquad (2\text{-}25)$$

Experiments conducted by Denington et al (Reference 2-4) using mercury and water have proven the validity of Equation 2-25. The results of their investigations, which included zero gravity tests, indicated that interfacial stability could be maintained in the presence of external disturbances by choosing appropriate tube diameters.

Using the above relation, it can be shown that the reference design radiator, having a tube diameter of 0.271 inches at the end of the condensing section, may experience interfacial instability during adverse accelerations exceeding 0.6 g.

Runback instability is the movement of slugs of condensate in the condensing tube toward the vapor header, resulting in pressure fluctuations and an unstable interface. This condition occurs when external body forces, opposing the direction of fluid flow, become greater than the vapor shear forces being exerted on the condensate film.

Denington et al (Reference 2-4) have investigated the mechanism of runback in vertical pipes for water in a one g environment. During stable condenser operation the wall shear force was assumed to be in the downward direction, but as runback occurs the wall shear force reverses direction. Therefore, it was reasoned that the point at which the wall shear force becomes zero is the runback point. From the

experimental data it was found that runback could be eliminated if the vapor velocity were greater than the critical velocity obtained from the following equation:

$$v_c = 308 \left(\rho_l \ \rho_v\right)^{1/2} \frac{D^2 g}{\mu_v} \qquad (2\text{-}26)$$

Using this approach, it can be shown that the design radiator can operate against an external acceleration of approximately 0.188 g without danger of runback.

Zero g instability is the emptying of the liquid condensate back into the vapor header due to a positive pressure gradient down the condensing tube. This condition is possible for short condensing length to diameter ratios and small momentum losses where the interface static pressure becomes larger than the inlet total pressure. Since the design condensing radiator has a static pressure drop of 3.78 lb/in^2 in the condensing tube section, this instability cannot arise.

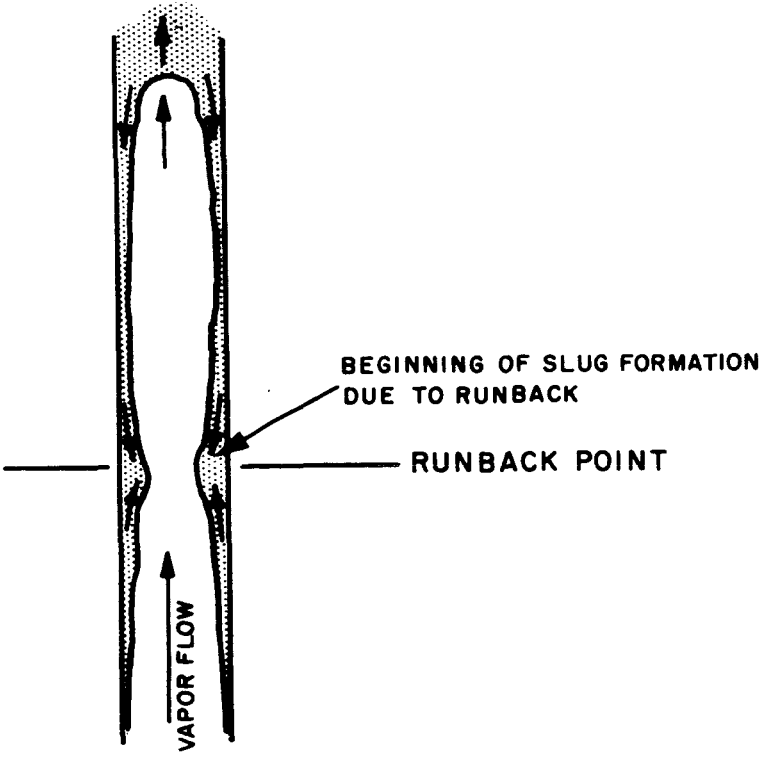

Figure 2-14. Runback Instability

Liquid leg instability results in the flow of vapor into the liquid header and liquid running back into the vapor header. This is a disastrous form of instability since the flow of vapor into the EM pump will make the system inoperable.

Liquid leg instability is caused by a larger pressure gradient in the liquid film than exists in the vapor. This condition can arise when external forces such as gravity create radial pressure differences between the annular condensate film and vapor. At the interface of the condensing and subcooling sections, the vapor and liquid interface pressure must be equal. Therefore, near the tube inlet the static pressure in the liquid leg will be higher than the pressure in the vapor. The liquid axial pressure gradient for a stable film can be given by:

$$\frac{dP_l}{dL} = \rho_l \left(g/g_c\right) \qquad (2\text{-}27)$$

The vapor axial pressure gradient can be calculated using the available correlations for two-phase flow.

For the design condensing radiator the static pressure gradient is 0.0312 (lb/in^2) /in. The liquid pressure gradient in the design radiator will exceed this when an opposing force greater than 1.29 g is present.

2.4.4 RADIATOR COMPUTER CODES

The comparison between the indirect and direct condensing radiators was performed with the aid of the Spartan III and V radiator optimization codes.

Since the singular purpose of Spartan III and V is the same, the basic considerations in obtaining an optimum design are similar for each of the programs. These considerations include the simultaneous solution of the meteoroid survival, thermal and fluid flow requirements, while optimizing toward a minimum system weight with the

possibility of an added constraint. The constraint may be an area limit, pump work limit, pressure drop limit or some combination of these.

The following is a list of input and output common to both Spartan III and V:

INPUT

- Thermal Requirements - heat rejected, inlet temperature, fluid temperature drop
- Mission Requirements - life, reliability
- Environmental Factors - Meteoroid size, density, flux, incident heat fluxes, view factors
- Physical Property Data - densities, Youngs' Moduli, viscosities, conductivities, etc.
- Configuration - different fin tube designs, various header, and feed line designs
- Geometric Factors - numbers of panels, tubes, tube spacing fin thickness, etc.
- Criteria for - pressure drop, heat transfer, meteoroid armor and bumper effects

OUTPUT

- Flow Characteristics - velocities, Reynolds number, pressure drop, pump work
- Temperature Characteristics - header and tube temperatures, fin temperatures and efficiencies, sink temperature
- Weights - fins, tubes, headers, liner, armor, fluid, etc.
- Geometry - projected radiator area, armor thickness, vulnerable area, tube length

Other significant features of the SPARTAN codes are as follows:

- The optimization process is performed by a separate "logic" subroutine which can perturb up to 20 inputs simultaneously to obtain a minimum system weight case.
- Capability to include the system weight penalty associated with pump work in the optimization.

- All or any fraction of the fin may be credited as bumper armor and the liner as integral armor for meeting meteoroid armor requirements.
- Temperature drops across the film, liner and armor are accounted for.
- Pressure drops include friction, turning and expansion and contraction losses.
- Panels may have common hot and cold headers.
- Armor may be preferentially located, as may be the case of a radiator in the shape of an open split cylinder.
- Fraction of the tube and header vulnerable area may be excluded from the armor calculations if otherwise protected, as by tankage. The vulnerable area of the tubes and headers may be based on the inside, outside or any intermediate area.
- Analyses include effect of radiation interchange between fin and tube for central fin tube heat rejection.

Spartan V was developed by GE-MSD over the past year specifically to design minimum weight direct condensing radiators. The code includes in detail the effects of two-phase flow on radiator feed line, header and matrix design from thermal and fluid dynamic aspects. The design criteria incorporated into Spartan V, including meteoroid criteria, fin-tube-header geometries, weight calculations and optimization procedure are completely consistent with Spartan III in order to achieve as accurate a comparison as possible.

The analysis presented in the Spartan V program considers the panel to be the radiator basic "building block." This consists of an inlet and outlet header connected by flow tubes; the flow tubes are separated by conduction fins. Due to the large variation in fluid density from tube inlet to outlet, the flow tubes are assumed to be divided into a tapered two-phase fluid section and a straight subcooling portion. In addition to radiator panels, the program has the capacity to consider inlet and outlet feed lines in calculating radiator loop pressure drop, armor requirements and weight. This is an important consideration for several reasons. Due to feed line effects, radiator inlet temperature, pressure and quality can change drastically from turbine exit conditions; also, inlet feedlines can comprise a significant fraction of the total vulnerable area.

The significant features of the Spartan V code which differ from Spartan III are listed below:

- Incremental condensing tube pressure drop which includes frictional, momentum and expansion and contraction losses
- Use of a modified Lockhart-Martinelli two-phase flow pressure drop correlation which includes liquid-vapor interface effects
- Calculation of condensing heat transfer coefficients and condensate film, liner and armor temperature drops
- Tapered condensing tubes
- Subcooled liquid tube section
- Bimetallic fin option
- Different size inlet and outlet headers and feed lines

All design radiators were obtained by using the optimization routine included in the Spartan codes. For the indirect cycle radiators the Spartan III code optimized the fluid temperature drop, number of tubes per panel, inside tube diameter, fin thickness and feed line diameter. In comparing the different combinations of redundant panels, the following assumptions or inputs were included in Spartan III:

a. At the end of mission lifetime the surviving panels have the capability to reject the specified waste heat without changing cycle conditions. For example, if 2 of 4 panels survive, the system was designed to reject twice the heat at start-up.

b. For design simplicity cylindrical headers were used as opposed to the lighter parabolic header design. In order to avoid maldistribution, the headers were sized so as to give a negligible pressure drop as compared to tube pressure drop.

c. None of the radiators were area limited.

d. Stainless steel tube liners 0.028 inches thick

e. Stainless steel header liners 0.020 inches thick

f. Fluid velocity in headers was limited to one half the fluid velocity in the tubes.

For the direct condensing radiator the weight was optimized by varying the number of panels, number of tubes per panel, fin thickness, condensing tube taper, inlet feed

line diameter and pressure drop from turbine exit to vapor-liquid interface. The assumptions made in Spartan V were the same as those in Spartan III except for those listed below, which accommodate the two-phase flow process:

1. Adiabatic two-phase flow in the inlet feed lines
2. Parabolic inlet and outlet headers
3. The smallest return feed line was limited to a 1 inch diameter. This criteria was found to limit the pressure drop in the return feed lines to an order of magnitude lower than that necessary to cause "flashing" of the sub-cooled liquid.

2.5 REFERENCES

2-1 Cockfield, R.D., "Comparison of Load Bearing and Non-Load Bearing Radiators for Nuclear Rankine Systems," NASA CR-72307, May 6, 1967.

2-2 Loeffler, I.J., S. Lieblein, and N. Clough. "Meteroid Protection for Space Radiators," ARS Paper 2543-62, September, 1962.

2-3 Larson, J.W., "Research on Spacecraft and Powerplant Integration Problems--Spacecraft Analysis Topical Report," NASA CR-54159, July 24, 1964.

2-4 Cockfield, R.D., "Definition of Spacecraft and Radiator Interrelations for Nuclear Rankine Systems," NASA CR-72245, January 26, 1967.

2-5 Denington, R.J., et al, "Space Radiator Study," Thompson Ramo Woolridge Inc., ASD Technical Report 61-697, April, 1962.

2-6 Haller, H.C., "Analysis of a Double Fin-Tube Flat Condenser-Radiator and Comparison With A Central Fin-Tube Radiator," NASA TN D 2558, 1964.

2-7 Krebs, R., Haller, H., and Auer, B., "Analysis and Design Procedures for a Flat, Direct-Condensing, Central Finned-Tube Radiator," NASA TN D-2472, 1964.

2-8 Stone, R.A., "Radiators for SNAP-50/SPUR," AiResearch Manufacturing Co., Technical Report AFAPL-TR-64-143, March, 1965.

2-9 Sawochka, S.G., "Thermal and Hydraulic Performance of Potassium during Condensation Inside a Single Tube," NASA CR-851, August, 1967.

2-10 Ewing, C.T., et al, "High Temperature Properties of Potassium," U.S. Naval Research Laboratory, NRL 6233, September 24, 1965.

2-11 Dukler, A.E., "Fluid Mechanics and Heat Transfer in Vertical Falling-Film Systems," Chemical Engineering Progress Symposium Series, No. 30, Vol. 56, 1960.

2-12 Lockhart, R.W. and Martinelli, R.C., "Proposed Correlation of Data for Isothermal Two-Phase, Two-Component Flow in Pipes," Chemical Engineering Progress, Vol. 45, No. 1, 1949.

2-13 McMillan, H.K., Fontaine, W.E., and Chaddock, J.F., "Pressure Drop in Isothermal Two-Phase Flow--A Modification of the Lockhart-Martinelli Correlation," ASME Paper 64-WA/FE-4, November, 1964.

2-14 Gutierrez, O.A., Sekas, N.F., Acker, L.W., and Fenn, D.B., "Potassium Condensing Tests of Horizontal Multitube Convective and Radiative Condensers Operating at Vapor Temperatures of 1250 to 1500°F," AIAA Specialists Conference on Rankine Space Power Systems, CONF-651026, October, 1965.

2-15 Heiskala, V.H., Smith, R.C., Elliott, E.A., Lancet, R.T., "Mercury Rankine (SNAP-2) Radiator Condenser Development Experience," AIAA Specialist Conference on Rankine Space Power Systems, CONF-651026, October, 1965.

2-16 Lamb, H., Hydrodynamics, sixth edition, Cambridge University Press, London, 1932, p. 370.

2-17 Tong, L.S., "Boiling Heat Transfer and Two-Phase Flow," John Wiley and Sons, Inc., New York, 1965.

3. RADIATOR COMPARISON

3.1 SPACECRAFT DESCRIPTION

The spacecraft concepts used as a basis for the radiator types compared in this study are shown in Figures 3-1 and 3-2. The spacecraft configuration used in both cases is consistent with the results of the first two tasks performed under this contract. That is, the arrangement of components and shielding requirements are appropriate to an unmanned interplanetary probe mission, and the radiators are non-deploying, load bearing, and conical in shape. The half-cone angle is chosen as 10 degrees to minimize shield weight and launch loads. The primary radiator supports all other components of the power system during launch. The power conversion equipment is located in a sealed unit, supported by a conical structure from the top of the primary radiator. The secondary, or auxiliary cooling radiator, surrounds the power conversion equipment and supports the reactor and shield. During launch, a small aerodynamic fairing covers the reactor and shield.

Since the launch vehicle is assumed to be a three-stage Saturn V, the payload must mate with the 260-inch diameter of the S-IVB stage. For the direct condensing radiator, the area required for heat rejection is less than that available on a cone with a 10-degree half-angle. A payload section, which includes the electric propulsion, communications, and navigation and control systems is attached to the base of the radiator and acts as an adapter section to the launch vehicle interface. The indirect condensing radiator used for comparison, shown in Figure 3-2, has an area that conveniently matches the area available on the conical section. The payload section for this concept is a cylindrical section and can therefore be made in any convenient length.

The size and shape required for the payload section depends on the particular mission requirements. Therefore, no weight implications can be drawn from the more convenient area match of the indirect condensing system radiator.

To keep the header length close to an optimum value, the radiator must be divided into a number of panels, which must always be a multiple of the number of independent loops. For the non-redundant systems compared in Reference 3-1, it was not necessary to divide the area into panels of equal area, since all panels were connected in a single loop. Instead, the tube lengths in each panel were held constant, close to the optimum value. For the redundant systems considered in this study, however, the individual loops must be of equal heat rejection capability, that is, the panels must be of equal area. To fit equal area panels on a conical surface, it is necessary to use unequal tube lengths. For example, in Figure 3-2, the upper bay is 191 inches in length and the lower bay is 146 inches in length. As a result, the radiator panel weights are greater for the lower bay than for the upper bay and therefore, reflect a tube length that is further from the optimum value. However, these weight differences are insignificant and generally vary less than 2 percent from one bay to another. Therefore, the detailed parameters for each radiator (Tables 3-1, 3-2, and 3-4) are listed only for the upper bay.

In the discussion of two-phase stability, it was noted that the reference design condensing radiator would experience runback instability under the influence of an adverse acceleration greater than 0.188 g's. For electrically propelled, unmanned interplanetary probe missions, accelerations typically will not exceed 10^{-4} g. However, some applications of nuclear potassium Rankine systems may require the power system to operate under acceleration conditions for which instability is a problem. To avoid adverse accelerations, the vapor headers are placed at the top of each bay, as shown in Figure 3-1. This arrangement introduces the problem of a temperature gradient across the bay joint. Excessive thermal stresses would occur if this joint were not designed in order to permit differential radial expansion between the two bays. Similar thermal gradient problems occur at the joints between the primary and secondary radiators and between the primary radiator and the payload section. Concepts for joints of this type are discussed in Reference 3-2. An alternative solution is to use a single bay for the condensing radiator and pay the weight penalty for an off-optimum tube length.

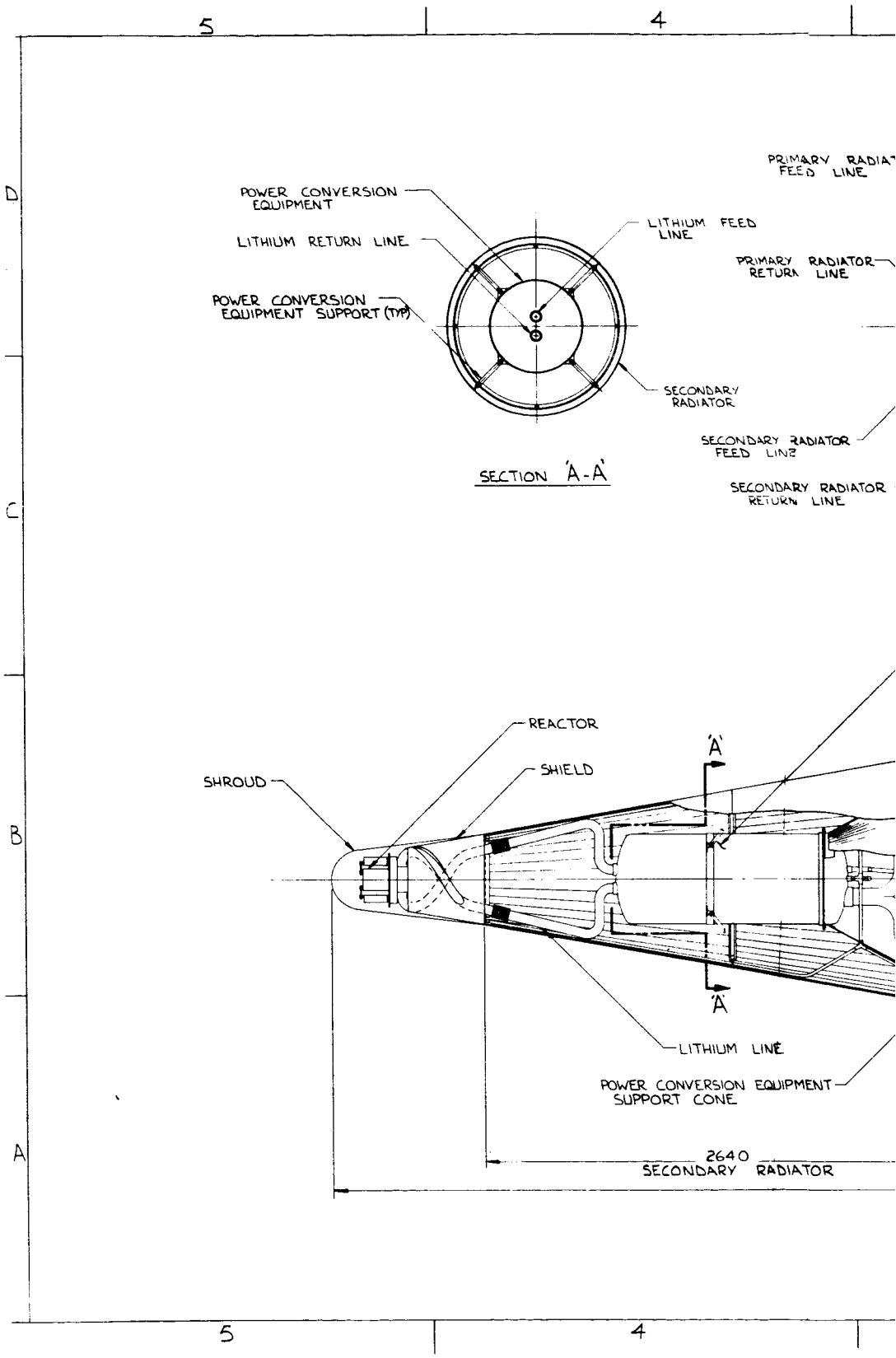
5
4
D
C
B
A
POWER CONVERSION EQUIPMENT
LITHIUM RETURN LINE
POWER CONVERSION EQUIPMENT SUPPORT (TYP)
LITHIUM FEED LINE
SECONDARY RADIATOR
SECTION 'A-A'
PRIMARY RADIAT
FEED LINE
PRIMARY RADIATOR RETURN LINE
SECONDARY RADIATOR FEED LINE
SECONDARY RADIATOR RETURN LINE
REACTOR
SHIELD
SHROUD
'A'
'A'
LITHIUM LINE
POWER CONVERSION EQUIPMENT SUPPORT CONE
2640
SECONDARY RADIATOR
5
4

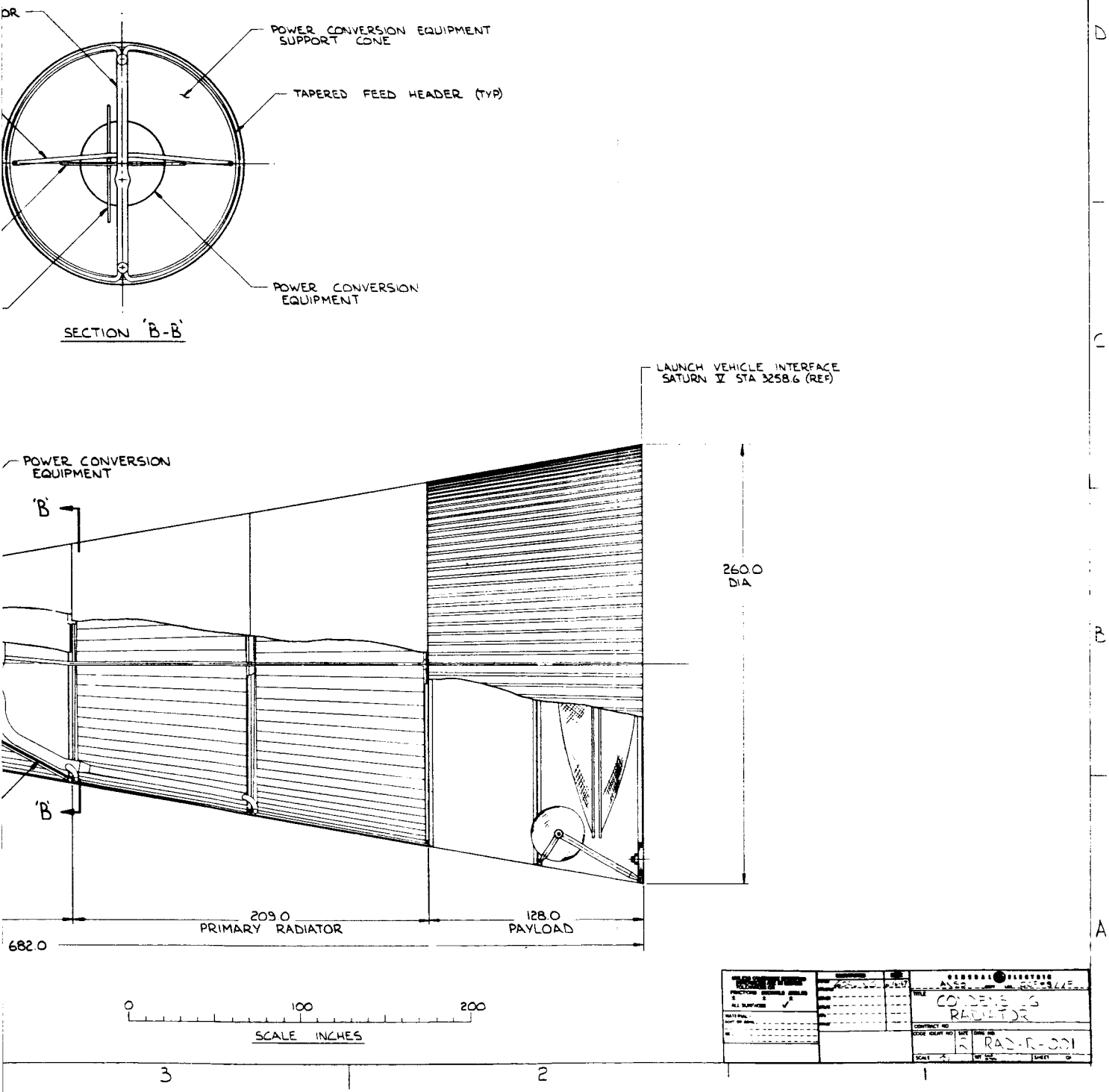

Figure 3-1. Spacecraft Configuration-Direct Condensing Radiator

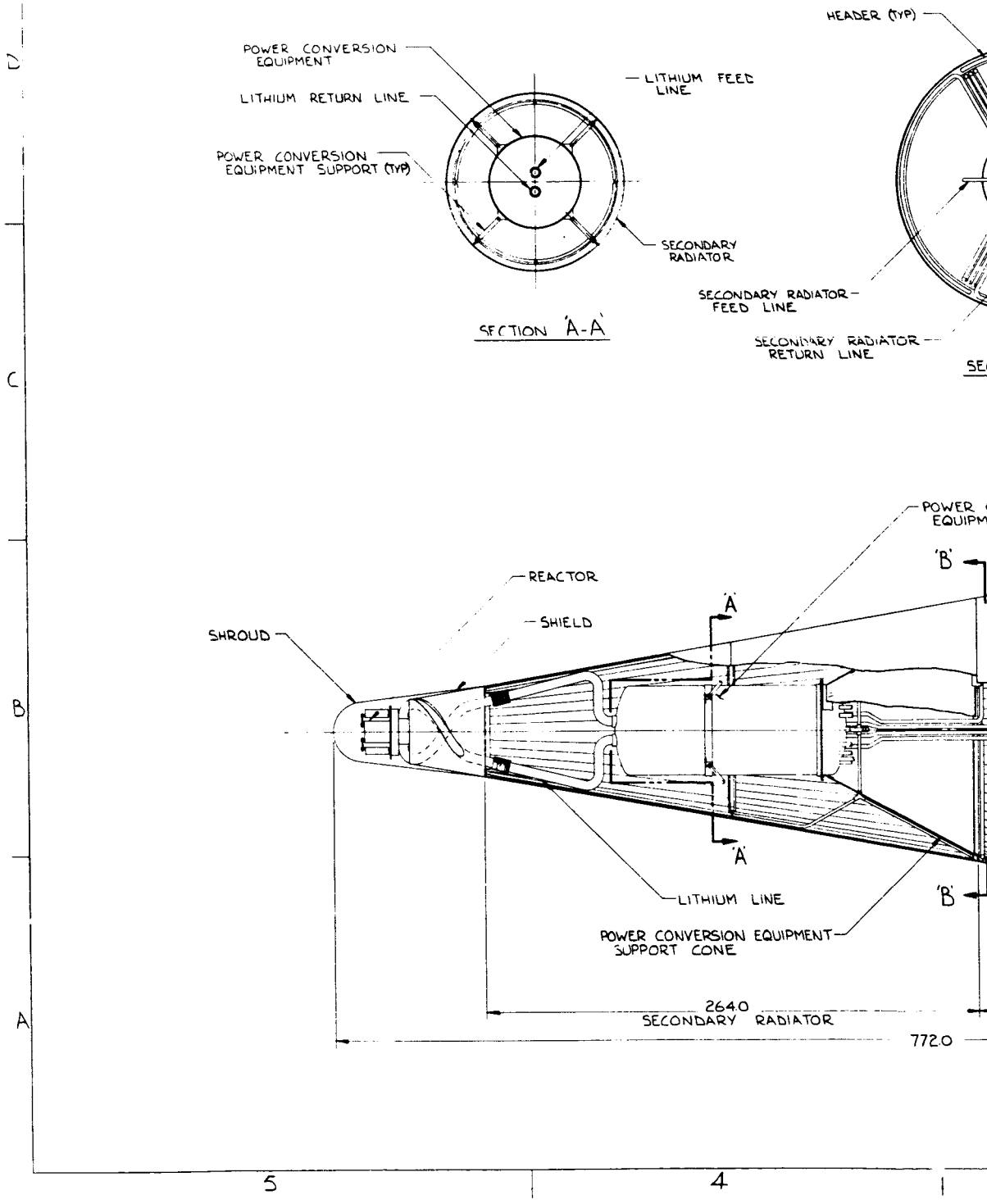
5
4
D
C
B
A
POWER CONVERSION EQUIPMENT
LITHIUM RETURN LINE
POWER CONVERSION EQUIPMENT SUPPORT (TYP)
LITHIUM FEED LINE
SECONDARY RADIATOR
SECTION 'A-A'
HEADER (TYP)
SECONDARY RADIATOR FEED LINE
SECONDARY RADIATOR RETURN LINE
REACTOR
SHIELD
SHROUD
'A'
'B'
LITHIUM LINE
POWER CONVERSION EQUIPMENT SUPPORT CONE
264.0
SECONDARY RADIATOR
772.0

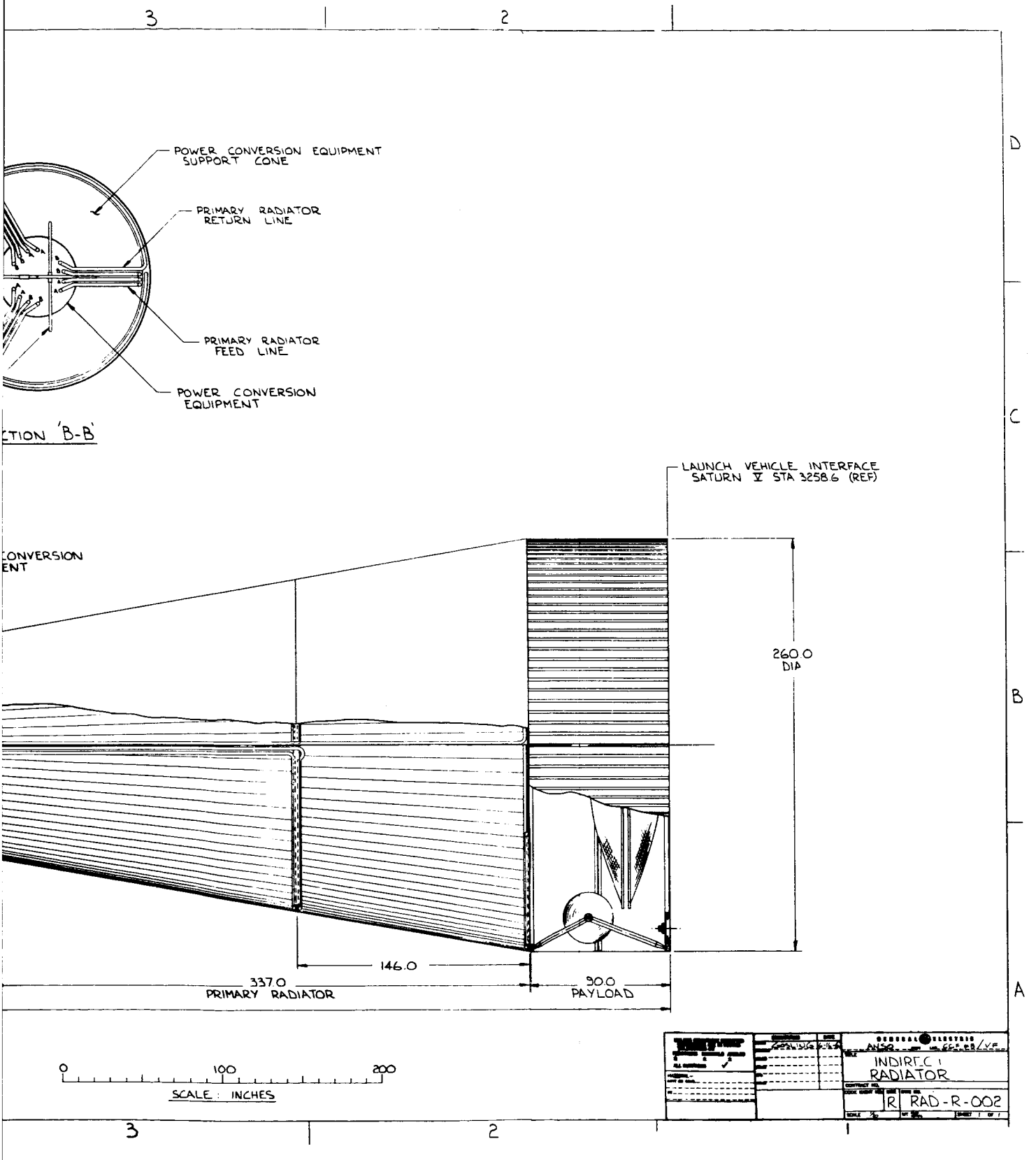

Figure 3-2. Spacecraft Configuration-
Indirect Condensing Radiator

3.2 STARTUP CONSIDERATIONS

The problem of startup has been recognized as one of the major unresolved problems in the development of Rankine system radiators and condensers (Reference 3-2). Consideration of the startup procedures may be the deciding factor in the selection of direct or indirect condensing radiator systems. Although startup of a nuclear system is a complex systems problem, certain aspects pertaining only to the heat rejection system can be considered independently. Although a separate and thorough study of startup considerations is beyond the scope of this study, some discussion of the startup problem has been included in this study to identify the key factors.

The primary concern for the heat rejection loop is to avoid coolant freezing. This is of less concern in the other components of the power system because the fluid inventory is smaller and can be packaged to conserve heat loss. The liquid metal coolants suitable for use in the primary heat rejection loops have melting temperatures in the same range of temperature that might be expected in space prior to startup. The indirect condensing radiator, using NaK with a melting temperature of 12°F, clearly is less susceptible to freezing than the direct condensing radiator using potassium, with a melting temperature of 147°F. Figure 3-3 shows the variation in effective sink temperature with absorptance and emittance for various configurations and orientations. The incident solar flux, earth emission and albedo of a 260 n. mi. orbit were assumed. It can be seen that radiator equilibrium temperatures above the melting temperature of NaK can be achieved with appropriate selection of α and ϵ. For example, a cylindrical radiator with its axis normal to the solar flux and parallel to the earth horizon (curve B), has an effective sink temperature of 140°F when $\alpha = 0.85$ and $\epsilon = 0.9$. These values of absorptance and emittance are typical of presently available iron titanate plasma sprayed coatings, suitable for use at 1300°F. The penalty on thermal performance at operating temperature is negligible, as shown in Figure 3-4. The effective sink temperature represents the average equilibrium temperature that the radiator would approach. However, without rotation, severe circumferential temperature gradients can exist, as shown in Figure 3-5. This suggests that it will be necessary to provide a slow rotation of the radiator about its axis to prevent freezing. An additional safety margin on coolant

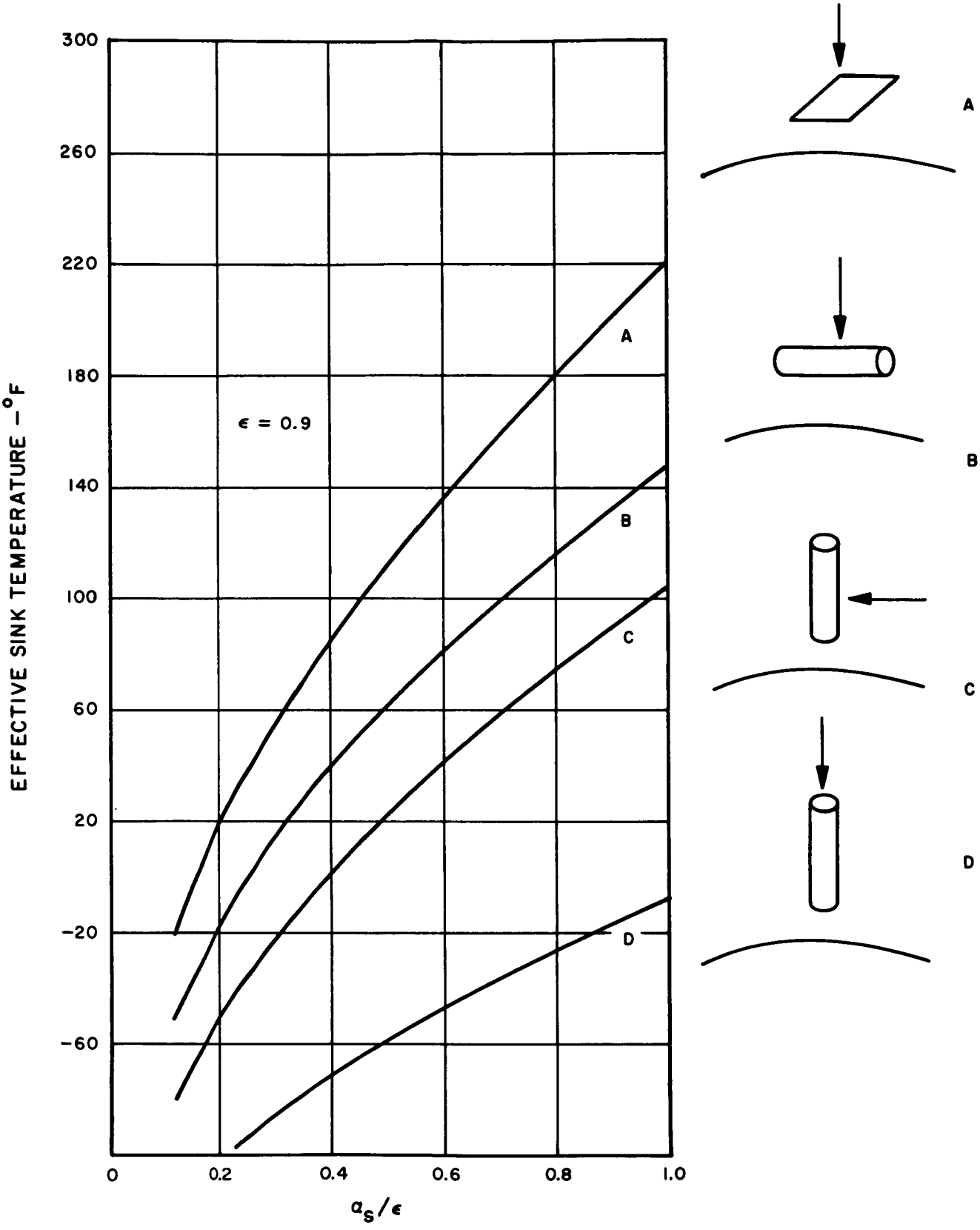

Figure 3-3. Effect of Radiator Surface Properties on Effective Sink Temperature

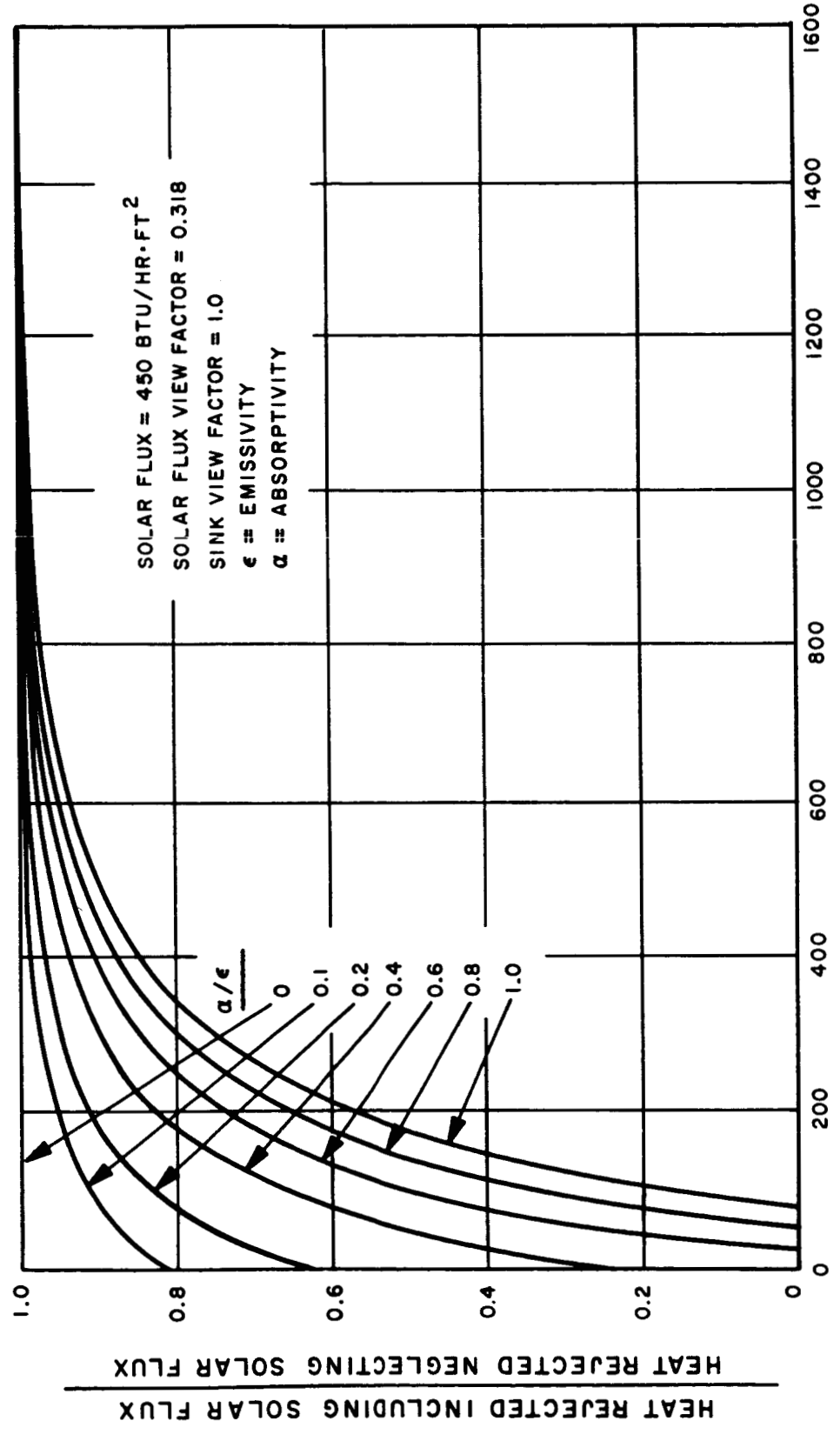

Figure 3-4. Effect of Radiator Surface Properties on Heat Rejection Capability

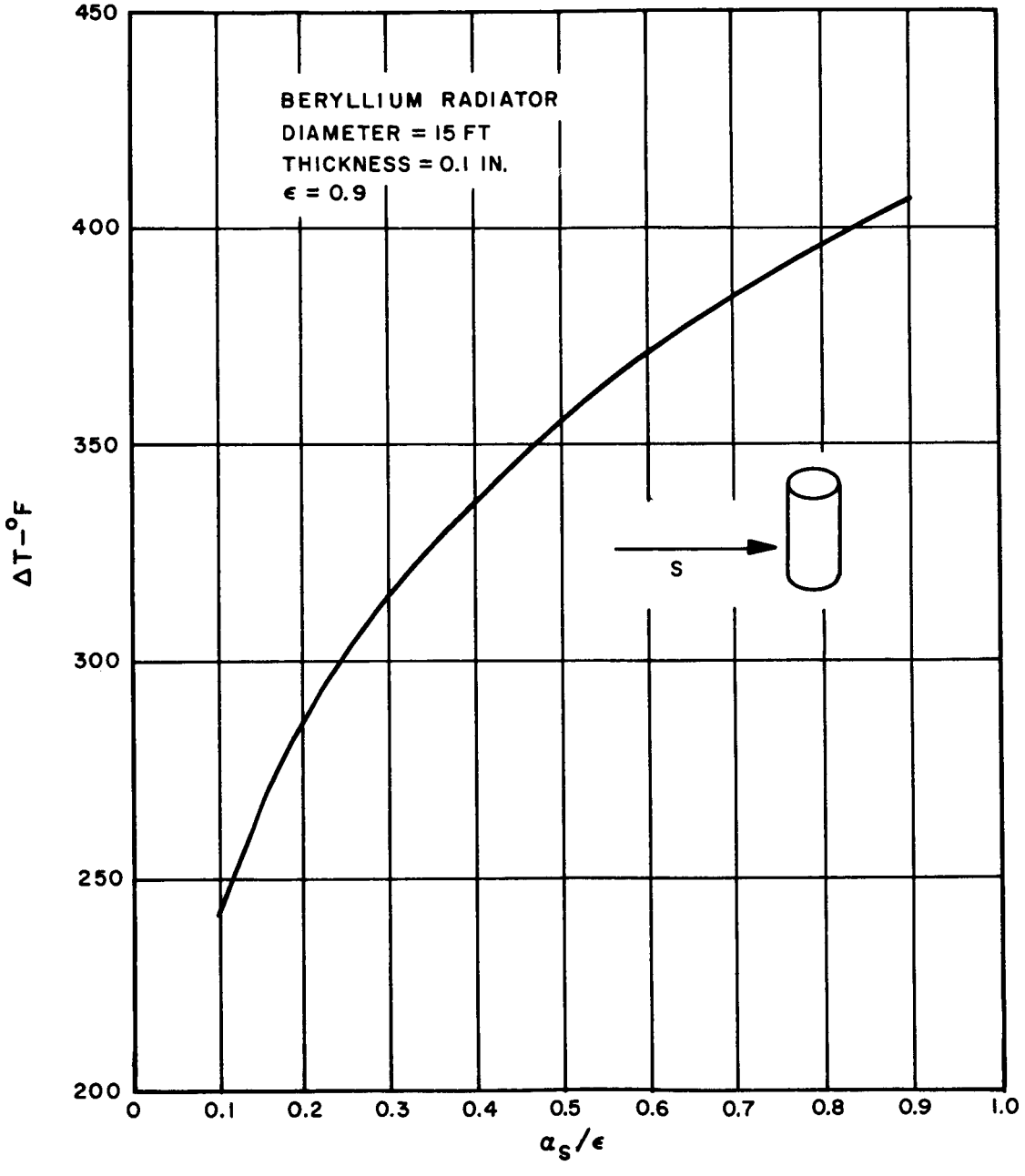

Figure 3-5. Circumferential Temperature Gradient on an Unheated Cylindrical Radiator

freezing may be obtained by using a tertiary alloy with a lower melting temperature, at the expense of some penalty in thermal performance. (References 3-4, 3-5) In any event, it appears that the startup problems associated with an indirect condensing radiator, using NaK coolant, can be resolved and that the solutions would also be applicable to power system shutdown and restart.

The startup problems of the direct condensing radiator, however, are more difficult. Figure 3-3 indicates that solar heating cannot be relied upon to maintain the radiator temperature above the melting temperature of potassium if the radiator is cylindrical in configuration. A flat panel configuration oriented normal to the solar flux (curve A) permits sufficiently high temperatures, but this implies a non-load bearing concept with a resulting structural weight penalty. The alternatives are to use a heat source or removable insulation to reduce heat losses, or some combination of both. Whereas the indirect condensing radiator can be launched filled with fluid, the direct condensing radiator would be launched "dry", with the potassium injected at the time of power system startup. This means that the circulation of the coolant through the radiator cannot be used to preheat or maintain the radiator at temperature. A separate heating network would therefore be required. The weight of an electrical heater covering all fluid passages would be prohibitive. Radioisotopes are attractive as heat sources, but a pumped coolant distribution system would be required. Pyrotechnic heating has also been proposed as a solution (Reference 3-6). The choice of preheating systems may be determined by the necessity for multiple start capability.

The energy requirements for preheating can be significantly reduced or eliminated entirely by providing insulation over the radiator surface. This insulation would then be removed at the time of startup.

The requirement to provide insulation on the radiator during launch is somewhat inconsistent with the concept of using the radiator as a load-bearing component. The insulation must withstand aerodynamic forces and have sufficient stiffness to avoid dynamic response (flutter). If the insulation is stiff generally as well as locally, it then carries all aerodynamic loads and becomes a primary load path. An examination of startup requirements is therefore essential to reaffirm conclusions on the merits of load-bearing versus non-load-bearing radiators. Under certain circumstances, it is

possible to provide a lightweight system of insulation and avoid the launch load problems. In Reference 3-7, a concept was discussed for a multiple use thermal shroud which took advantage of rotation to deploy and eject the insulation.

3.3 REFERENCE DESIGN RADIATORS

This section discusses the results of the radiator analyses, and identifies the reference designs used for comparison. For the indirect condensing system radiators, it was found that significant weight reductions could be obtained by the use of redundancy at the highest survival probabilities considered. Redundancy for the direct condensing radiators was not considered, since this would involve system concepts beyond the scope of this study.

Figure 3-6 shows the effect of redundancy on the weight of the radiator for the indirect condensing system. The redundancy is described in terms of the number of independent loops required for full power heat rejection capability, compared with the number of loops provided. Cases were analyzed for four, six, eight, and twelve loops. The weight saving realized is a result of a reduction in armor and fin weight. (Note that for the cylindrical radiator configuration, the fin contributes significantly to the armor protection.) However, as the degree of redundancy increases, the increased radiator area offsets the reduction in armor weight. This is illustrated in Figure 3-6, where it can be seen that the 5/6 case is lighter than either 3/4 or 4/6. An additional effect is that, as the number of loops provided increases, the additional feed line weight offsets the reduction in armor weight. Hence in Figure 3-6, 7/8 is not significantly lighter than 5/6, and 11/12 is definitely heavier. In Table 3-1, detailed parameters have been listed for each of the optimum redundant cases: 3/4, 5/6, 7/8, and 10/12.

Figure 3-6 also shows that the optimum redundancy changes with survival probability. As survival probability is changed from 0.9 to 0.99, and 0.999, the lightest redundant radiator weight is achieved with 3/4, 5/6 and 7/8 loops surviving, respectively.

The effect of redundancy can be seen by comparing the detailed parameters listed in Table 3-2 for 5/6 loops surviving and 6/6 loops surviving. The 30 percent difference

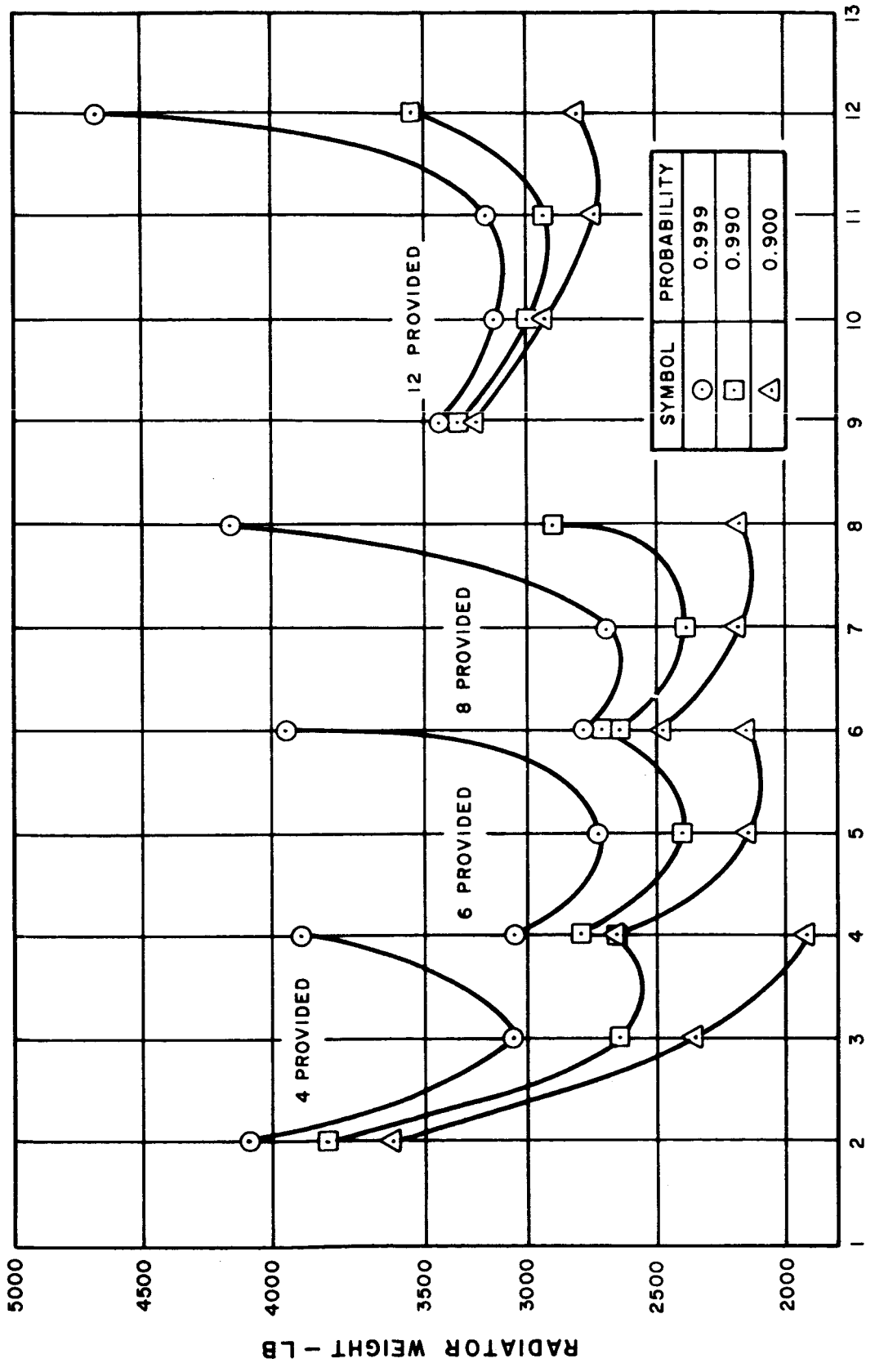

Figure 3-6. Effect of Redundancy on Radiator Weight for the Indirect Condensing System

TABLE 3-1. SUMMARY OF LIGHTEST WEIGHT RADIATORS
(OVERALL SURVIVAL PROBABILITY = 0.999)

LOOPS SURVIVING/TOTAL NO. OF LOOPS		3/4	5/6	7/8	10/12
*Total Heat Rejected	(kW)	2460	2460	2460	2460
Radiator Weight	(lb)	3052	2712	2687	2925
Radiator Area	(ft^2)	1709	1528	1441	2023
Inlet Fluid Temperature	($^\circ F$)	1300	1300	1300	1300
Fluid Temperature Drop	($^\circ F$)	390	380	390	460
Number of Panels		4	6	8	12
Number of Tubes/Panel		78	55	41	40
Header Length	(ft)	21.6	14.4	10.8	12.4
Tube Length	(ft)	19.3	17.3	16.4	13.3
Inside Tube Diameter	(in.)	0.206	0.194	0.192	0.180
Inside Header Diameter	(in.)	2.57	2.03	1.74	1.61
Fin Thickness	(in.)	0.066	0.064	0.064	0.042
Fin Length	(in.)	1.48	1.40	1.41	1.71
Fin Efficiency	(%)	77.7	79.2	78.8	67.0
Total Vulnerable Area	(ft^2)	1156	1075	1027	1210
Required Armor Thickness	(in.)	0.309	0.304	0.303	0.21
Tube Armor Thickness	(in.)	0.050	0.051	0.050	0.033
Weight of Armor	(lb)	592	537	494	369
Weight of Fins	(lb)	1067	927	876	805
Weight of Tubes	(lb)	1080	972	899	820
Weight of Headers	(lb)	371	247	190	288
**Weight of Feed Lines	(lb)	535	566	710	1013
Hydraulic Pump Power	(kW)	4.14	3.77	3.40	3.48
Smallest Feed Line Dia	(in.)	2.4	2.3	2.15	1.95

* This value refers to the end-of-life condition when loop failure has occurred.

** The feed line weight includes the weight of the fluid.

TABLE 3-2. EFFECT OF REDUNDANCY ON RADIATOR WEIGHT
(OVERALL SURVIVAL PROBABILITY = 0.999)

LOOPS SURVIVING/TOTAL NO. OF LOOPS		5/6	6/6	2/2*
Heat Rejected	(MW)	2.46	2.46	2.46
Radiator Weight	(lb)	2712	3917	3597
Radiator Area	(ft^2)	1528	1117	1077
Fluid Inlet Temperature	($^\circ F$)	1300	1300	1300
Fluid ΔT	($^\circ F$)	380	270	250
Number of Panels		6	6	8
Number of Tubes per Panel		55	33	29
Header Length	(ft)	14.4	14.4	12.2
Inside Tube Diameter	(in.)	0.194	0.246	0.258
Inside Header Diameter	(in.)	2.03	2.00	1.96
Total Vulnerable Area	(ft^2)	1075	958	898
Required Armor Thickness	(in.)	0.305	0.780	0.768
Tube Armor Thickness	(in.)	0.0507	0.170	0.164
Fin Thickness	(in.)	0.0640	0.172	0.172
Fin Efficiency	(%)	79	77	78
Tube Length	(ft)	17.3	12.6	10.7
Smallest Feed Line Inside Diameter	(in.)	2.3	2.4	1.3
Radiator Loop ΔP	(psi)	24.9	21.7	11.6
Feed Line ΔP	(psi)	10.6	9.65	4.33
Coolant Flow Rate	(lb/sec)	34.4	40.4	43.6
Hydraulic Pump Power	(kW)	3.77	3.86	2.23
Pump Penalty	(lb/kWe)	125	125	200
Weight of Feed Lines	(lb)	566	507	251
Weight of Headers	(lb)	171	164	261
Weight of Tubes	(lb)	972	1361	1348
Weight of Fins	(lb)	927	1810	1737
Weight of Armor	(lb)	537	1119	1094

* From Reference 3-1

in weight can be attributed to the reduction in armor thickness from 0.780 inches to 0.305 inches. Table 3-2 also shows the parameters for the indirect condensing system radiator used in the structural comparison of Reference 3-1. It can be seen that for non-redundant radiators, the lightest weight is achieved with the fewest number of independent loops. The penalty paid for redundancy is increased radiating area. Table 3-2 shows that the radiator with 5/6 loops surviving requires 37 percent more area than the radiator with 6/6 loops surviving. For the launch vehicle limitations considered in this study, this increased area has no adverse effects. However, if the area available were less than the area required for optimum design, the weight penalty could offset any gains from redundancy. This effect is important in extrapolating the results to higher power levels. In order to retain the advantageous armor reduction afforded by redundancy when area limitations become critical, it may be desirable to consider concepts such as utilization of the upper launch vehicle stages or deployable radiators.

In order to make a system weight comparison, the pump weight, pump power weight penalty, and the condenser weight must be added to the radiator weight for the indirect condensing system. These weights may also have an influence on the selection of optimum redundancy arrangement.

The pump weights for each radiator are obtained as a function of flow rate and pressure drop, using the approximate relation shown in Figure 3-7. The weights shown in this figure are estimated from data presented in Reference 3-8. The conclusion drawn in Reference 3-8, which covers a survey of various pump types and configurations, is that ac induction pumps are the best choice for space nuclear systems. Although lighter by as much as a factor of 2.5, dc conduction pumps are eliminated because of reliability considerations.

The pump power weight penalty was specified as 25 lb/kWe. This penalty represents the increase in the entire power system weight in order to provide the additional pump power. It may be observed in Table 3-3 that the penalty has a minimum value when eight loops are provided.

The condenser weight is assumed to be 200 pounds for all the systems considered. This weight is estimated by scaling the condensers described in Reference 3-2. Although

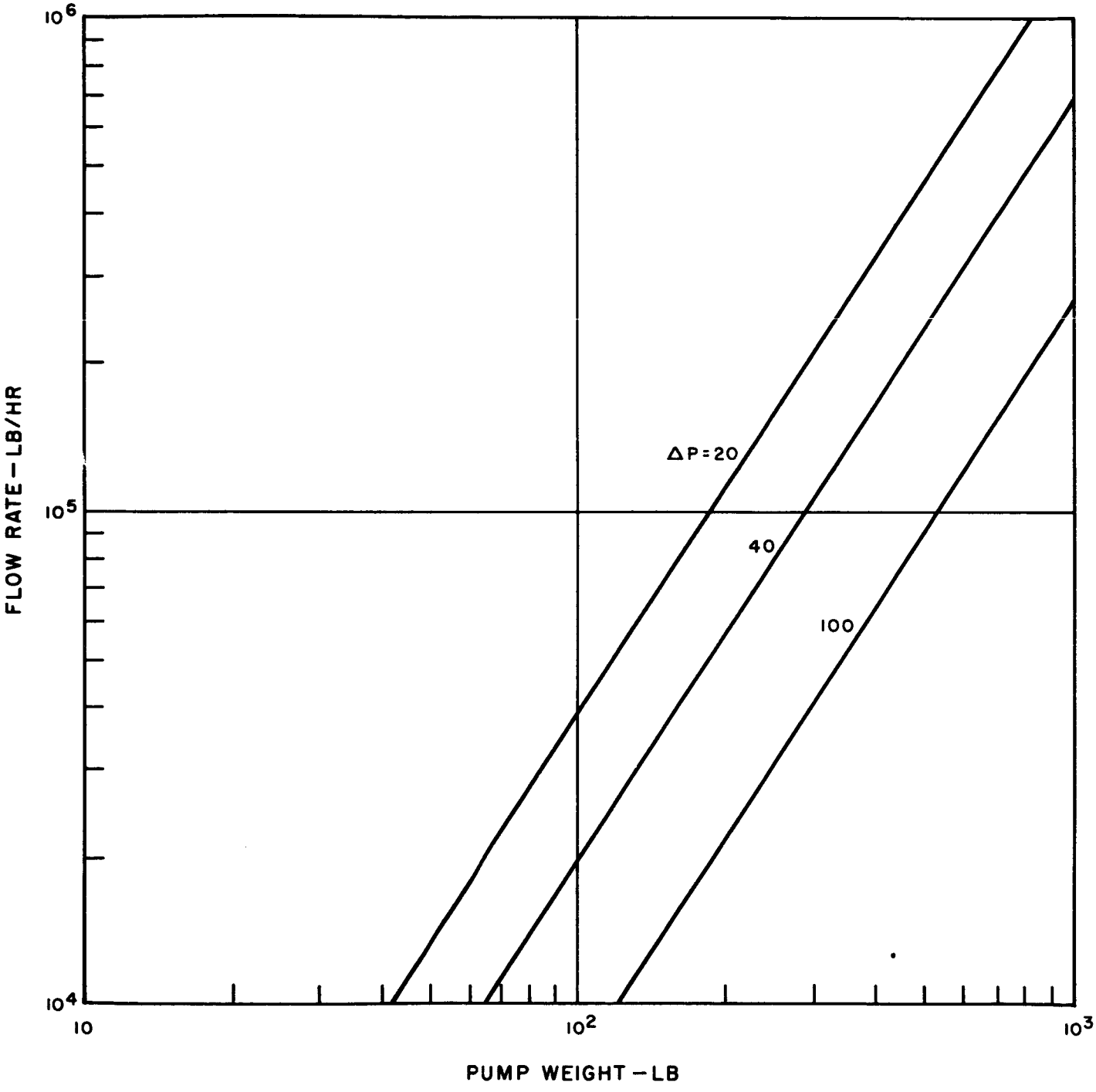

Figure 3-7. Weight of AC Induction Pumps

TABLE 3-3. SUMMARY OF INDIRECT SYSTEM COMPONENT WEIGHTS
(SURVIVAL PROBABILITY = 0.999)

LOOPS SURVIVING/LOOPS PROVIDED	3/4	5/6*	7/8	10/12
Radiator Weight	3050	2710	2690	2920
Pump Weight	410	440	470	540
Pump Power Weight Penalty	520	470	430	440
Condenser Weight	200	200	200	200
Total Weight	4180	3820	3790	4100

*Reference Design Radiator

there is some argument for increasing the condenser weight as a function of the number of heat rejection loops provided, the weight is more strongly a function of the condensing surface area required, which is approximately constant.

Table 3-3 shows the effect of considering the additional heat rejection system components. The result is that 7/8 loops have the lightest redundancy arrangement by a margin of less than 1 percent. Although pump reliabilities are not considered explicitly in this study, it seems reasonable to conclude that the elimination of two pumps in choosing 5/6 rather than 7/8 loops is worth this small penalty.

The direct condensing radiator has the advantage of system simplicity in eliminating the need for a condenser-heat exchanger and heat rejection loop pumps. The higher effective radiating temperature of the direct condensing radiator significantly reduces the required heat rejection area. The smaller surface area becomes an important consideration when area limitations are approached.

Although redundancy is not considered, two different panel arrangements for the direct condensing radiator are included in the study. Figure 3-8 shows the weights for four- and eight-panel configuration, for survival probabilities of 0.999, 0.99 and 0.9. The four panel configuration has a single bay, with tubes running the full length of the radiator. The radiator weights are plotted against the static pressure drop in the vapor

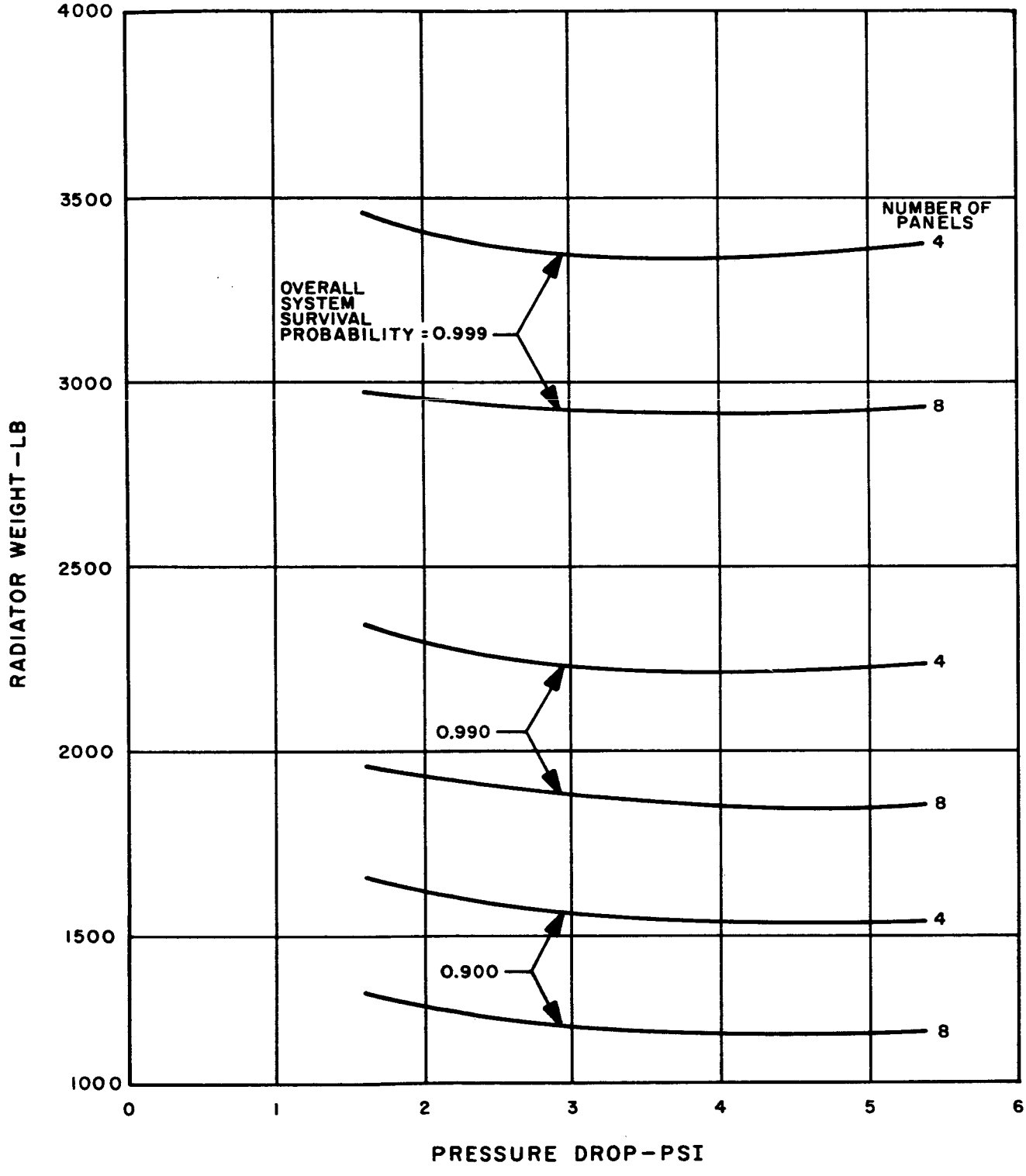

Figure 3-8. Effect of Pressure Drop on Condensing Radiator Weight

section of the radiator loop, which is actually a measure of the temperature drop from turbine exit to the point of complete condensation. The effect of increasing the pressure drop in the condensing tube section is to reduce tube diameter and vulnerable area, but also to lower the effective radiating temperature. The overall effect is to make the radiator weight insensitive to pressure drop for the conditions investigated.

The eight-panel configuration chosen as the reference design has inlet headers located at the top of each bay (Figure 3-1). As discussed previously, this arrangement would be required for missions in which the operating radiator would be subjected to an axial acceleration greater than 0.188 g. This arrangement has the disadvantage of placing a large thermal gradient across the joint between bays, and thus requires provisions for relative radial expansion. The weight penalty of such an expansion joint is not included in the comparison of this study since there are relatively few missions where accelerations of this magnitude would be experienced. An alternative to the expansion joint would be to use a single bay, as indicated by the four-panel configuration. The weight penalty of a single bay arrangement is indicated by the comparison shown in Table 3-4. This penalty would increase rapidly with increasing power level as the tube length increased further from the optimum.

To show the influence of the tube taper on radiator weight, data were generated with the Spartan V code for variations of the reference design radiator. Figure 3-9 shows the relationship between radiator weight, tube taper, and inside tube diameter at tube outlet. The choice of taper and outlet tube diameter is determined mainly by minimizing the vulnerable area per tube while satisfying the pressure drop constraint.

Although the feed line design is a major consideration in any space radiator design, the two-phase flow radiator system is more sensitive to pressure drop variations in both the inlet and outlet feed lines. The higher the inlet feed line pressure drop, the lower the effective radiator temperature in the condensing section. The variation of weight and radiator inlet fluid temperature with changing feed line diameter is shown in Figure 3-10. for the condensing radiator. The feed line diameter refers to the smallest diameter in the inlet feed line network which occurs at the feed line-inlet header joint. At a feed

TABLE 3-4. CONDENSING RADIATOR COMPARISON
(SURVIVAL PROBABILITY = 0.999)

		8 PANEL*	4 PANEL
Heat Rejected	(MW)	2.46	2.46
Radiator Weight	(lb)	2920 **	3346
Radiator Area	(ft^2)	815	798
Inlet Fluid Quality	(%)	83.8	83.8
Fluid Temperature at Feed Line Inlet	($^\circ$F)	1350	1350
Fluid Temperature at Vapor-Liquid Interface	($^\circ$F)	1275	1275
Fluid Temperature at Radiator Exit	($^\circ$F)	1100	1100
Number of Tubes per Panel		24	22
Header Length	(ft)	9.17	9.17
Inside Tube Diameter at Inlet	(in.)	0.458	0.749
Inside Tube Diameter at Outlet	(in.)	0.271	0.448
Inside Vapor Header Diameter at Inlet	(in.)	3.17	4.97
Inside Liquid Header Diameter at Outlet	(in.)	1.88	2.97
Total Vulnerable Area	(ft^2)	806	852
Required Armor Thickness	(in.)	0.780	0.799
Tube Armor Thickness	(in.)	0.155	0.151
Fin Thickness	(in.)	0.185	0.195
Fin Efficiency	(%)	80	79
Length of Condensing Section	(ft)	10.1	19.9
Length of Sub-cooling Section	(ft)	0.60	1.18
Smallest Inlet Feed Line Diameter	(in.)	3.3	3.4
Smallest Outlet Feed Line Diameter	(in.)	1.0	1.0
Inlet Header Vapor Velocity	(ft/sec)	253	209
Inlet Tube Vapor Velocity	(ft/sec)	504	417
Weight of Feed Lines	(lb)	159	167
Weight of Condensing Tube Section	(lb)	1223	1570
Weight of Sub-cooling Tube Section	(lb)	62	80
Weight of Fins	(lb)	1402	1457
Weight of Vapor Headers	(lb)	27	21
Weight of Liquid Headers	(lb)	47	51
Weight of Armor	(lb)	1043	1299

* Reference Design Radiator

** Does not include weight penalty for expansion joint between bays.

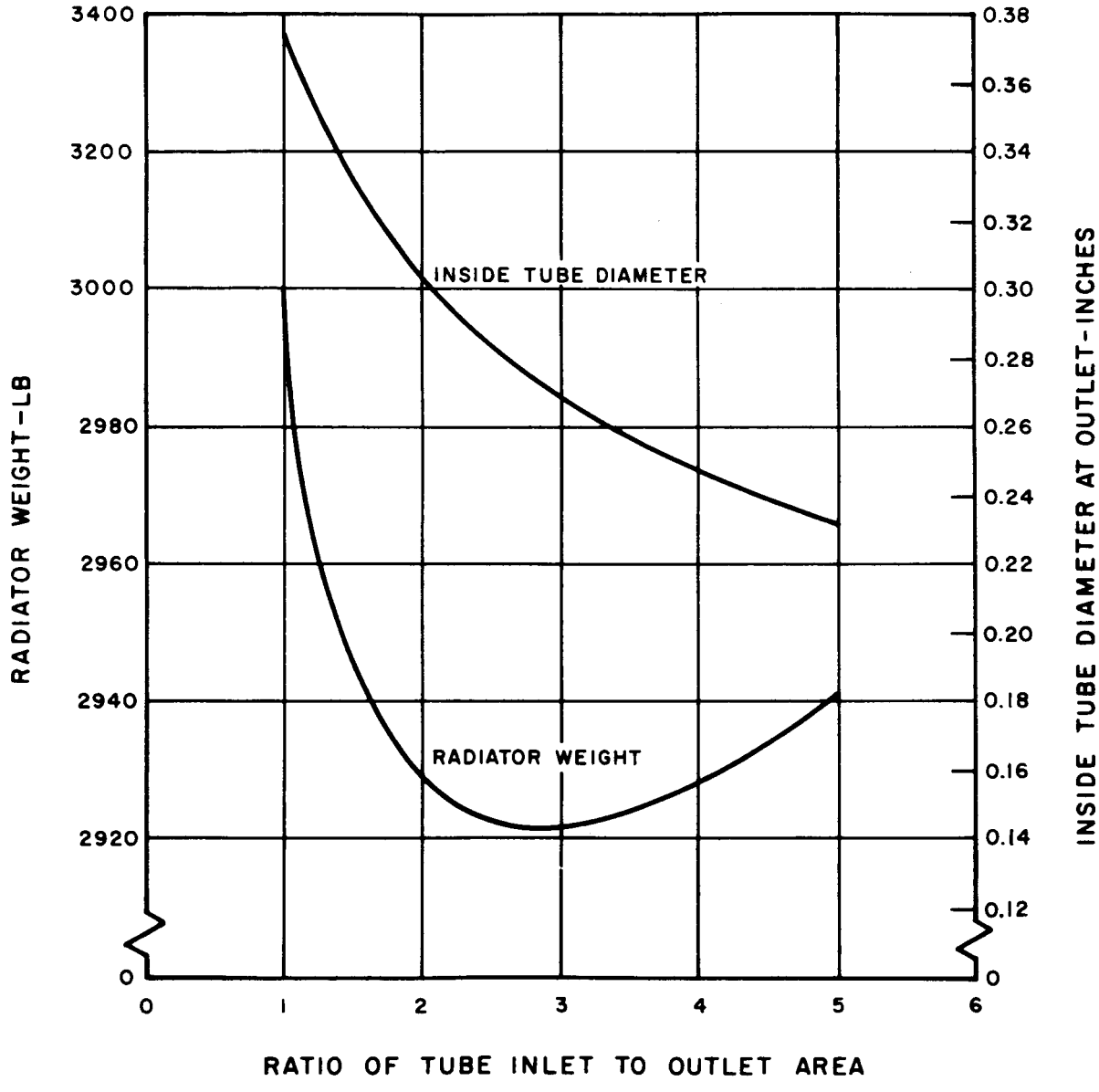

Figure 3-9. Effect of Tube Taper on Condensing Radiator Weight

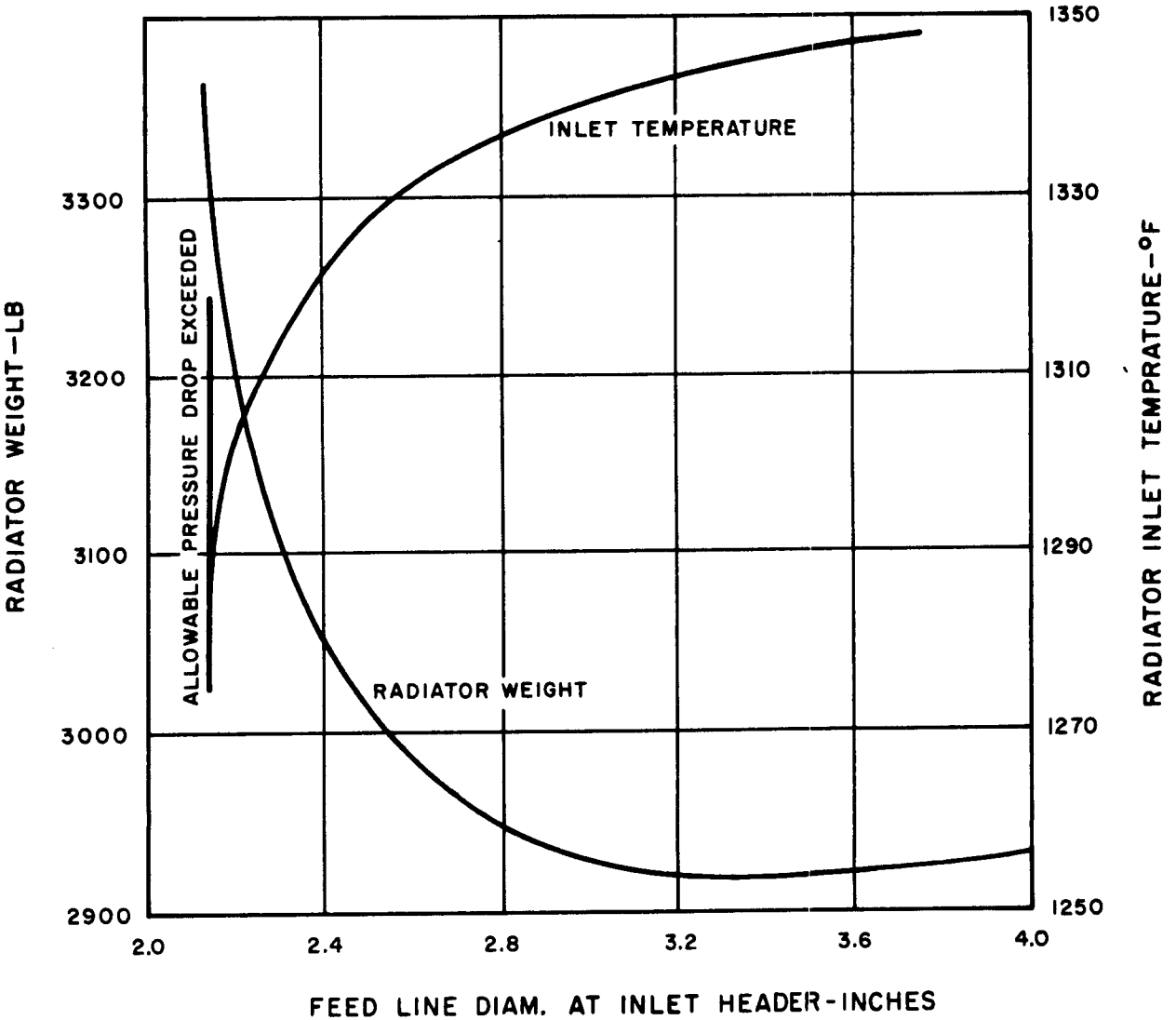

Figure 3-10. Effect of Feed Line Diameter on Radiator Weight

line diameter less than 2.14 inches, the feed line pressure drop is greater than that allowed in the entire vapor section of the radiator loop. Feed line diameters larger than 3.3 inches result in a weight increase due to the effects of vulnerable area and the weight of the feed line piping and fluid.

One aspect of the design direct condensing radiator which deserves examination is the temperature history of the fluid from the point of turbine exit to the point of return to the EM pump (See Figure 3-11). The two-phase fluid enters the inlet feed line from the turbine at a temperature of 1350° F, a static pressure of 11.9 psi and a quality of 83.8 percent. Adiabatic flow is assumed in the feed lines. The static pressure drop in the inlet feed lines causes the fluid temperature to decrease to 1344° F at the radiator inlet; this flow process results in a slight change in fluid quality (83.9 percent at radiator inlet). The potassium then enters the inlet headers which are assumed to be situated beneath the radiating surface.

In the condensing portion of the radiator tubes, the potassium temperature decreases to 1275° F as a result of the static pressure drop. The frictional pressure drop, which can be less than the momentum pressure rise for this type of system, is increased by the tube taper. The tapered tube insures a negative pressure gradient in the condensing tube section which promotes flow stability and also offers a slight weight advantage.

One characteristic of the direct condensing radiator is the large axial temperature gradient in the fluid in the subcooling portion of the tube. This is due to the low mass flow rates, high fluid temperature, and generally low sink temperatures involved. For the direct condensing radiator under consideration, the fluid undergoes a temperature drop from 1275° F to 1100° F over a distance of 7.1 inches. This characteristic demands that the condensing and subcooling lengths be accurately predicted for proper cycle operation.

The subcooled liquid enters the exit headers and return feed lines to the jet pump. No heat is assumed to be rejected over this portion of the loop. Examination of Figure 3-11 shows that the pressure at the EM pump has been kept conservatively high to insure against cavitation.

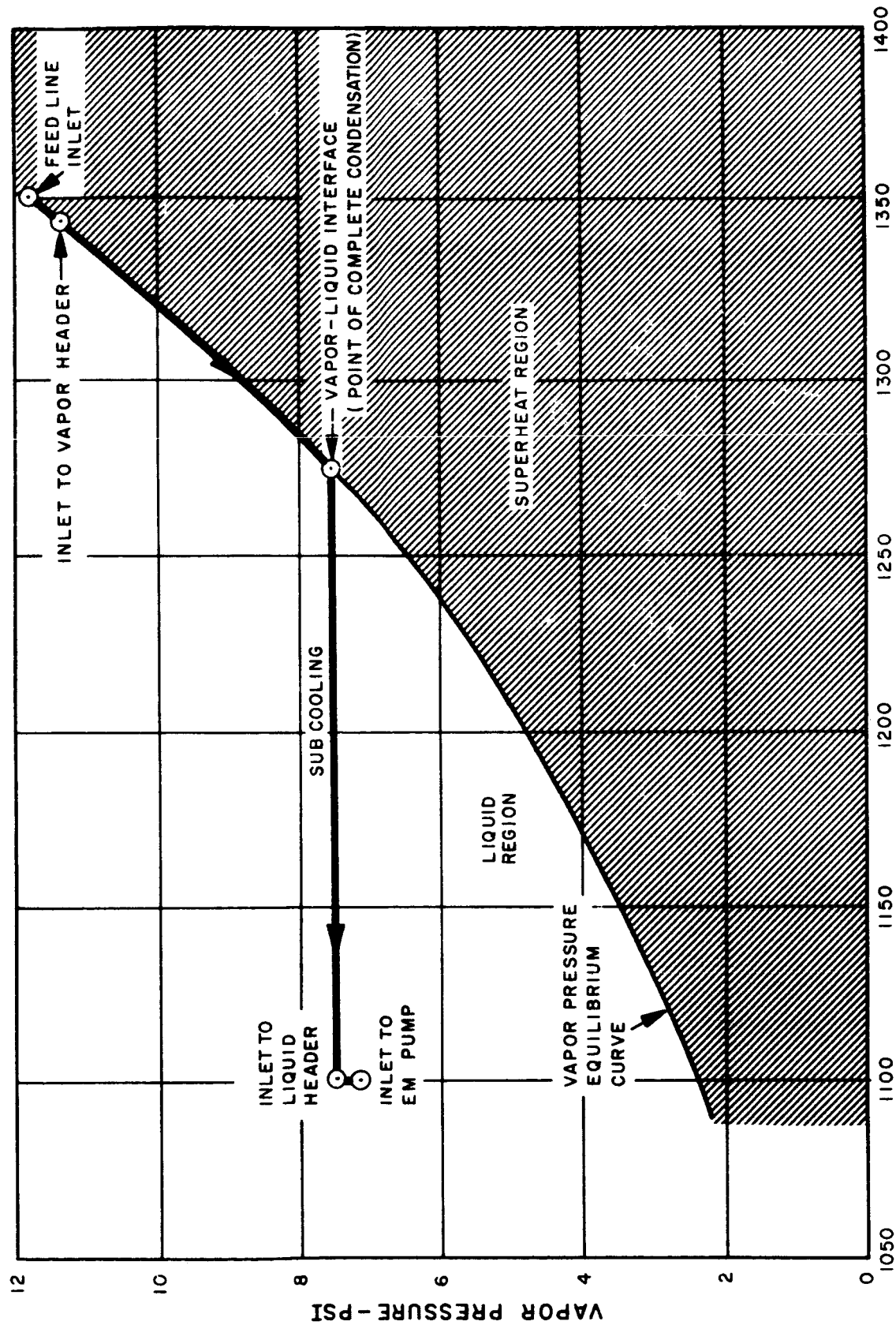

Figure 3-11. Temperature-Pressure History for Condensing Radiator

The rapid subcooling which occurs in the radiator tubes can produce disastrous results when flow maldistribution is present. Severe maldistribution can change the axial temperature drop from tube-to-tube to the extent where radiator buckling is caused by the induced thermal stresses. Direct condensing radiator tests using potassium, conducted at Oak Ridge National Laboratory by A. P. Fraas (Reference 3-9), exhibited maldistribution due to "sonic velocities in the vapor manifold." The fluid velocities in the vapor header for the condensing radiators presented here are limited to one-half the vapor velocity at the tube inlet; this gives the header the same characteristics as a plenum. This design criteria is used for both the indirect and direct condensing radiator parametric studies. The header vapor velocity for the eight-panel condensing radiator design is 252 ft/sec. The equilibrium sonic velocity for saturated potassium at 1340°F is given by W. D. Weatherford Jr. (Reference 3-10) as 1443 ft/sec. Therefore, flow maldistribution would not be expected to occur in the eight-panel condensing design radiator or in any of the other radiators designed in this study.

3.4 WEIGHT COMPARISON

The direct condensing radiator has a weight advantage over the indirect condensing system for all conditions considered in this study. Figure 3-12 compares the weights for survival probabilities of 0.9, 0.99, and 0.999. The weight additions to the indirect system for pumps, pump power penalty, and condenser are essentially constant over the range of probabilities. The most significant effect is in the radiator weight. Whereas the direct condensing radiator weight increases by 140 percent as probability increases from 0.9 to 0.999, the indirect system radiator weight increases by only 42 percent. This difference in sensitivity can be attributed to the ability of the indirect system radiator to take advantage of the effects of redundancy. The trend indicated in Figure 3-12 suggests that at nonpenetration probabilities above 0.999 and/or lifetimes greater than five years, the weight advantage of the direct condensing radiator continues to diminish and at some point the indirect system becomes lighter.

Although the effect of power level was not a part of this study, some inferences can be drawn from the data presented. As discussed earlier, the indirect system radiator,

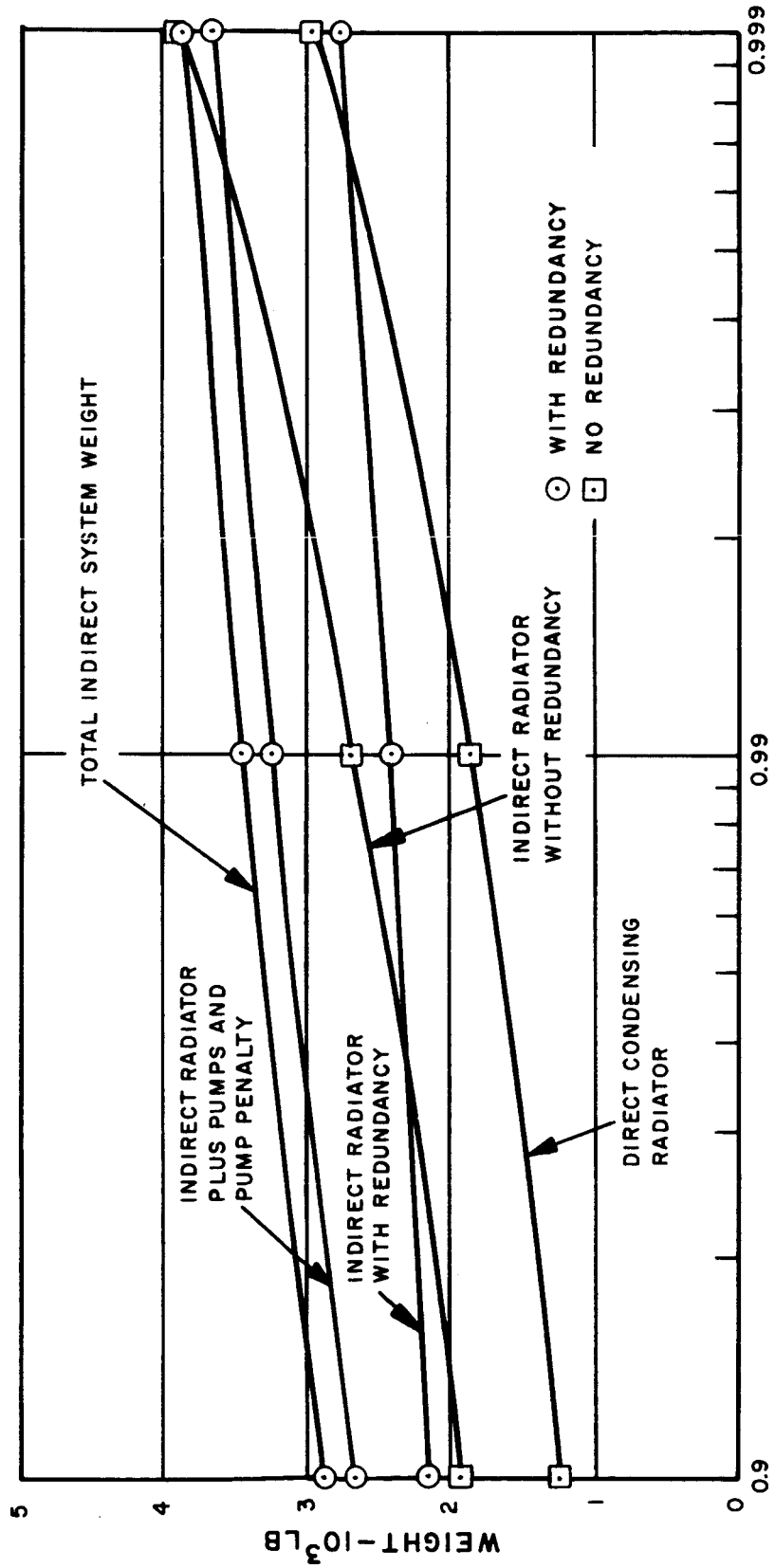

Figure 3-12. Effect of Survival Probability on Radiator Comparison

being significantly larger in area, is more sensitive to the envelope limitations of the launch vehicle. This sensitivity is magnified when the indirect system employs redundant loops. A secondary effect of the larger area is an increase in feed line length. Hence, the feed line weight for the indirect system radiator is 21 percent of the total radiator weight. The direct condensing radiator has shorter feed lines and gains from the very low mass flow rate of the coolant. As a result, the feed line weight for the direct condensing radiator is only 5.5 percent of the total radiator weight. As the power level of the system increases, the influence of the feed lines increases. For example, in Reference 3-1 the following was noted:

Power level (kWe)	300	1200
Feed line weight (lb)	251	1354
Feed line pump penalty weight (lb)	289	3066

That is, for a power level increase by a factor of four, the feed line weight and pump power penalty attributable to the feed lines, increase by a factor of eight.

Hence, the area limitation effects and feed line weights indicate that the direct radiator will increase its weight advantage at increasing power levels. However, a compensating factor favors the indirect system. Increased power level has approximately the same effect on armor thickness as increased survival time. Figure 3-12 indicates that a more severe meteoroid protection criteria would favor the indirect system. However, this effect is not likely to offset the factors favoring the direct condensing radiator.

Load-bearing radiator concepts were chosen for all the radiators considered in this study because of the advantages shown in the comparison reported in Reference 3-1. As a result, structural weight is not an important factor in the comparison between indirect and direct condensing systems. Had non-load-bearing concepts been considered, the structural weight differences would have been a major factor. None of the radiators considered has a specific weight of tubes and fins less than 1.2 lb/ft^2. In Reference 3-11 it was shown that beryllium radiators of this density in a conical configuration have more than adequate structural capability to withstand the most severe launch loads of the Saturn V launch vehicle. Parasitic structural weight, which includes the weight of

brackets, insulation, fasteners, coatings, and so on, accounts for a small percentage of the total radiator weight, but it is not enough to influence the choice of radiator type. Since significant differences for the various radiators being compared cannot be identified, the parasitic structural weight has not been included in the total system weights listed.

3.5 REFERENCES

3-1 Cockfield, R. D., "Comparison of Load Bearing and Non-Load Bearing Radiators for Nuclear Rankine Systems," NASA CR-72307, May 6, 1967.

3-2 Larson, J. W., "Research on Spacecraft and Powerplant Integration Problems," Second Quarterly Report, GE Document No. 63SD886, October, 1963.

3-3 Lieblein, S., Introduction to Radiator and Condenser Session of AIAA Specialist Conference on Rankine Space Power Systems, CONF-651026, October, 1965.

3-4 Tepper, F., King, J., and Greer, J., "Multicomponent Alkali Metal Alloys," MSA Technical Report AFAPL-TR-65-73, July, 1965.

3-5 "Low Melting NaK-Cesium Alloys," MSA Report 62-106, September, 1962.

3-6 Lalli, V. R., "Pyrotechnics for Efficient Preheating of Space Power Systems," Space/Aeronautics, November, 1965.

3-7 Tharpe, B. J., "Study on Application of Nuclear Electrical Power to Manned Orbiting Space Station," NASA CR-54160, September, 1964.

3-8 Rhudy, R. G. and Verkamp, J. P., "Electromagnetic Alkali Metal Pump Research Program," NASA CR-380, February, 1966.

3-9 Fraas, A. P., "Design and Development Tests on Direct Condensing Potassium Radiators," AIAA Specialists Conference on Rankine Space Power Systems, October, 1964.

3-10 Weatherford, W. D., Jr., Tyler, J. C., and Ku, P. M., "Properties of Inorganic Energy-Conversion and Heat-Transfer Fluids for Space Applications," WADD Technical Report 61-96, November, 1961.

3-11 Cockfield, R. D., "Definition of Spacecraft and Radiator Interrelations for Nuclear Rankine Systems," NASA CR-72245, January 26, 1967.

4. CONCLUSIONS

The comparison made in this study is for load-bearing, beryllium radiators, applicable to a nuclear potassium Rankine system for an unmanned interplanetary probe mission, launched by a three-stage Saturn V. The power level is assumed to be 2.46 MW_t heat rejected, approximately equivalent to 300 kW_e net electrical power. Meteoroid nonpenetration probabilities of 0.9, 0.99, and 0.99 for a five year life are considered. Among the conclusions reached in this study are the following:

a. The direct condensing radiator has a significant weight advantage over the indirect condensing system for all conditions considered in this study. Extrapolation to more severe meteoroid protection requirements may favor the indirect system. Consideration of startup requirements, however, strongly favor the indirect system and may offset the apparent weight advantage of the direct condensing radiator.

b. The use of redundant loops in the indirect system provides a means of reducing overall radiator weight at the higher survival probabilities.

c. The indirect system radiator is considerably larger in area than the direct condensing radiator and is therefore sensitive to launch vehicle area limitations. This sensitivity is increased when panel redundancy is employed.

d. The weight advantage of the direct condensing radiator is accompanied by an increase in system reliability due to the elimination of pumps.

e. For the conditions considered in this study, where load-bearing radiators are employed, structural considerations do not influence the comparison between direct condensing and indirect systems.

f. Design of the direct condensing radiator is more critical due to the importance of avoiding two-phase flow instabilities and maldistribution.

g. Operation of the direct condensing radiator is sensitive to internal and external disturbances and adverse accelerations. For some missions, consideration of accelerations may influence the choice of flow direction through the tubes. The resulting adverse thermal gradient from one bay to the next implies a weight penalty for an expansion joint.

h. Although the effect of power level was not investigated, it would appear that the direct condensing radiator would retain its weight advantage over a wide range of power levels, if startup problems were ignored. The startup problems associated with the direct condensing radiator would be intensified at higher power levels.

i. The Spartan V computer code developed for the design of direct condensing radiators shows excellent agreement with the test data available for potassium.

5. NOMENCLATURE

A = area

C = constant used in Blasius equation

C_c = correction factor to Nusselt's relation

D = diameter

D_s = recommended stable diameter

E = energy

KE = kinetic energy

L = length

M = molecular weight

N_{Re} = Reynolds number

P = pressure

PE = potential energy

ΔP_f = frictional pressure drop

ΔP_m = momentum pressure drop

ΔP_{tp} = two-phase pressure drop

Q = heat transfer rate

R = universal gas constant

T = temperature

ΔT = temperature drop

V = velocity

W = flow rate

X = square root of the ratio of the liquid pressure drop to gas pressure drop assuming each phase to flow separately

f = friction factor as defined by the Blasius expression

g = acceleration

g_c = gravitational constant

h = heat transfer coefficient

h_c = condensing heat transfer coefficient

$\bar{h}_c$ = average condensing heat transfer from fluid inlet to point of complete condensation

k = thermal conductivity

m = exponent of Reynold's number in Blasius expression for friction factor for gas phase

n = exponent of Reynold's number in Blasius expression for friction factor for liquid phase

v = velocity

v_o = inlet vapor velocity

w = flow rate

x = length

GREEK LETTERS

α = absorptivity

δ = condensate film thickness

ϵ = emissivity

η = wave amplitude

η_o = maximum wave amplitude

θ = ratio of gas Reynolds to gas Weber number

λ = wavelength

μ = viscosity

ν = kinematic viscosity

ρ = density

σ = surface tension

σ_c = condensation coefficient, fraction of the molecules striking the surface which actually condense

σ_e = evaporation coefficient, fraction of the predicted molecular flux from the liquid surface which actually leaves the surface

φ_v = function of X used in calculating two-phase pressure drop

SUBSCRIPTS

c = critical

exp = experimental

f = condensate film or frictional

l = liquid phase

v = vapor phase